

People's Democratic Republic of Algeria
Ministry of Higher Education and Scientific Research
Mohamed El Bachir El Ibrahimi University of Bordj Bou Arreridj
Faculty of Mathematics and Informatics
Informatics Department



DISSERTATION

Presented in fulfillment of the requirements of obtaining the degree

Master in Informatics

Specialty: Business Intelligence

THEME

Brain Tumor Detection Using U-Net and SVM

Presented by:

BENGUEZZOU Mohammed

BENYAHIAOUI Mohamed Assil

Publicly defended on: 11/06/2025

In front of the jury composed of:

President: Dr. LAIFA Meriem

Examiner: Dr. REGOUID Meriem

Supervisor: Dr. ZOUAOUI Hakima

2024/2025

Dedication

To the architects of my dreams, my parents, whose unwavering love and guidance have been my compass; to my family, the sanctuary of my heart, and to my friends, the sparks of joy in my journey.

This thesis is a testament to your belief in me, a reflection of your sacrifices, and a celebration of the bond we share. Thank you for being my pillars of strength and my endless source of inspiration.

- Mohammed

Dedication

To my parents, whose steadfast love, support, and guidance have been the cornerstone of my dreams; to my family, my unwavering foundation and sanctuary; and to my friends, who fill my life with joy and laughter.

This thesis is a tribute to their dedication, a mirror of their faith in me, and a celebration of our shared journey. Thank you for being my strength and my endless source of inspiration.

- Assil

Acknowledgments

Above all, we would like to thank GOD for granting health, the possibility and the will to start and continue our studies.

We would first like to thank our supervisor, **Dr. Hakima Zouaoui**, for giving us the chance to do our research and for providing invaluable guidance throughout this research. Also, we would acknowledge her for her generosity, her kindness, her knowledge, the time she gave us and her great availability which she showed us; made our task a lot easier.

We would also like to express our thanks to the members of the jury who honored us by participating in the examination of this work and enriching it with their proposals **Dr. Laifa Meriem** and **Dr. Regouid Meriem**.

In addition, we would like to acknowledge our parents for their love, care, prayers, scarifies and for being always there for us

Abstract

Brain tumors, particularly gliomas, pose a significant clinical challenge, requiring both precise localization and accurate grading to guide treatment. Accurate segmentation of tumor regions is a critical first step, enabling meaningful analysis and interpretation of the affected areas. In this project, we present a hybrid framework that first segments tumor regions in brain Magnetic Resonance Imaging (MRI) scans using a U-Net model trained on the Brain Tumor Segmentation dataset, and then classifies these regions as Low-Grade or High-Grade Gliomas with a Support Vector Machine (SVM) model based on features extracted from the segmented masks. On the held-out test set, our U-Net achieved an accuracy of 99.3%, while the SVM classifier delivered an overall accuracy of 93%.

Keywords: Brain Tumor, U-Net, SVM, MRI, BraTS, Segmentation.

Résumé

Les tumeurs cérébrales, en particulier les gliomes, posent un défi clinique important, nécessitant à la fois une localisation précise et un classement précis pour guider le traitement. La segmentation précise des régions tumorales est une première étape essentielle, permettant une analyse et une interprétation significatives des zones touchées. Dans ce projet, nous présentons un cadre hybride qui segmente d'abord les régions tumorales dans l'imagerie par résonance magnétique (IRM) du cerveau en utilisant un modèle U-Net formé sur la base de données de segmentation des tumeurs cérébrales (BraTS), puis classe ces régions comme faibleGliomes de grade ou de haut grade avec un modèle SVM (Support Vector Machine) basé sur les caractéristiques extraites des masques segmentés. Sur l'ensemble de test non exécuté, notre U-Net a atteint une précision de 99,3 %, tandis que le classificateur SVM a fourni une précision globale de 93 %.

Mots-clés: Tumeur cérébrale, U-Net, SVM, IRM, BraTS, Segmentation.

ملخص

تُشكل أورام الدماغ، وخاصة الأورام الدبقية، تحدياً طبياً كبيراً، وتتطلب إلى التحديد والتصنيف بشكل دقيق من أجل توجيه العلاج. إن التقسيم الدقيق لمناطق الورم يعد خطوة أولى بالغة الأهمية، حيث يتيح إجراء تحليل وتفسير مفيد للمناطق المصابة. في هذا المشروع، نقدم إطاراً هجيناً يقوم أولاً بتقسيم مناطق الورم في عمليات مسح (MRI) للدماغ باستخدام نموذج (U-Net) المدرب على مجموعة بيانات أورام الدماغ (BraTS2020) ثم يقوم بتصنيف هذه المناطق على أنها أورام دبقية منخفضة الدرجة أو عالية الدرجة باستخدام نموذج آلة الدعم المتجه (SVM) استناداً إلى الميزات المستخرجة من الأقنعة المجزأة. في مجموعة الاختبار، حققت شبكة (U-Net) الخاصة بنا دقة قدرها 99,3%، بينما قدم مصنف (SVM) دقة إجمالية قدرها 93%.

الكلمات المفتاحية: أورام الدماغ، U-Net، SVM، MRI، BraTS، Segmentation.

Table of Contents

List of abbreviations	xi
List of Figures	xii
List of Tables	xiv
General Introduction	1
1 Medical and Technical Concepts	2
1.1 Introduction	2
1.2 The Microscopic Description of the Brain	2
1.3 Brain Tissue	3
1.4 Classification of Brain Tumors	4
1.4.1 Benign Tumors	4
1.4.2 Premalignant Tumors	5
1.4.3 Malignant Tumors	5
1.5 Common Intracranial Tumor Types	5
1.6 Signs and Symptoms Associated with Brain Tumors	6
1.7 Diagnosis of Brain Tumors	6
1.7.1 Physical Examination	6
1.7.2 Complementary Examination	6
1.7.3 Brain Biopsy	7
1.7.4 Medical Imaging	7
1.8 Medical Imaging in Brain Tumor Diagnosis	7
1.9 Conclusion	9

2	Deep Learning and Machine Learning	10
2.1	Introduction	10
2.2	What is Artificial Intelligence?	10
2.3	Machine Learning	11
2.3.1	Why Machine Learning?	12
2.3.2	Machine Learning Application Examples	13
2.3.3	Different Techniques and Algorithms in Machine Learning	13
2.3.4	Machine Learning approaches	14
2.4	Deep Learning	16
2.4.1	Why Deep Learning?	17
2.4.2	Deep Learning Application Examples	17
2.4.3	Different Architectures of Deep Learning	18
2.4.4	Convolutional Neural Networks (CNNs)	19
2.5	Conclusion	22
3	State of the art on Brain Tumor Detection methods	23
3.1	Introduction	23
3.2	Literature Review	23
3.2.1	Contemporary Methods for Tissue Analysis	23
3.2.2	Image processing techniques	26
3.3	Related Work	27
3.3.1	Brain Tumor Segmentation and Grading of Lower-Grade Glioma	27
3.3.2	Wavelet Statistical Texture + RNN	27
3.3.3	Hybrid CNN + NADE	28
3.3.4	Hierarchical Transfer Learning with AlexNet & GoogleNet	28
3.3.5	VGG Block-wise Fine-Tuning	28
3.4	Conclusion	29
4	Contribution	30
4.1	Introduction	30
4.2	Proposed Framework Overview	30
4.2.1	End-to-End Inference Pipeline	30
4.2.2	Models Training Workflow	35

4.3	Dataset and Preprocessing	36
4.3.1	BraTS Dataset Description	36
4.3.2	Dataset Splitting	37
4.3.3	Data Preprocessing	38
4.4	Evaluation Metrics	39
4.5	Results and Discussion	41
4.5.1	Segmentation Results	41
4.5.2	Classification Results	44
4.6	Application Demo	45
4.6.1	Upload Page	45
4.6.2	Results Page	46
4.7	Conclusion	47
	General Conclusion	48
	bibliography	48

List of abbreviations

AI Artificial Intelligence.

CAD Computer-Aided Diagnosis.

CNN Convolutional Neural Network.

CNS Central Nervous System.

CT Computed Tomography.

IOU Intersection Over Union.

ML Machine Learning.

MRI Magnetic Resonance Imaging.

NADE Neural Autoregressive Distribution Estimator.

RNN Recurrent Neural Network.

SVM Support Vector Machine.

WHO World Health Organization.

List of Figures

1.1	Brain main parts: cerebrum, cerebellum, brainstem, and diencephalon [1]. . . .	3
1.2	Segmentation of a brain MRI into gray matter (GM), white matter (WM), and CSF by Statistical Parametric Mapping (SPM) [2].	4
1.3	Example of brain MRI image. [3]	8
2.1	Differences between AI, machine learning, and deep learning. [4]	11
2.2	Illustration of the Machine Learning Process [5]	11
2.3	Illustration of the Supervised learning process [6]	15
2.4	Illustration of the Unsupervised learning process [6]	15
2.5	Illustration of the Reinforcement learning process [6]	16
2.6	Illustration of the Deep Learning Process. [5]	16
2.7	Convolutional Neural Network Architecture [7]	20
2.8	Convolution Layer in a Convolutional Neural Network [8]	21
4.1	Overview of the end-to-end inference pipeline.	31
4.2	U-Net Architecture Illustrating the Encoding and Decoding Arms with Skip Connections. [9]	32
4.3	Support Vector Machine (SVM) Decision Boundary Visualization	34
4.4	Overview of the training workflow.	35
4.5	Brats modalities: T1, T1ce, T2, and T2-FLAIR.	36
4.6	Segmentation of Tumor classes.	37
4.7	Dataset splitting: training, validation, and test sets.	38
4.8	Training and Validation Accuracy over Epochs for the U-Net Segmentation Model	42
4.9	Training and Validation Loss over Epochs for the U-Net Segmentation Model .	42

4.10 Training and Validation Dice Coefficient over Epochs for the U-Net Segmentation Model	43
4.11 Training and Validation Mean IoU over Epochs for the U-Net Segmentation Model	43
4.12 Sample of a Predicted tumor segmentation masks.	44
4.13 Confusion matrix for the SVM classifier.	45
4.14 Upload page of the application demo.	46
4.15 Results page of the application demo.	47

List of Tables

3.1	Summary of prior methods in brain tumor segmentation and classification . . .	29
4.1	Performance Metrics for the U-Net Segmentation Model	44
4.2	Performance Metrics of SVM Classifier on the Test Set	45

General Introduction

Brain tumors represent one of the most challenging conditions in modern medicine, with precise diagnosis and classification being crucial for effective treatment planning and patient outcomes.

Although magnetic resonance imaging (MRI) has revolutionized brain tumor visualization, the interpretation of these scans remains a complex, time-consuming task requiring specialized expertise. Radiologists must analyze hundreds of images per patient, identifying subtle patterns that differentiate tumor types and grades—a process susceptible to inter-observer variability and human fatigue. Recent advances in artificial intelligence, particularly in deep learning and machine learning, offer promising solutions to these challenges. Automated systems can potentially enhance diagnostic accuracy, reduce analysis time, and provide objective, reproducible assessments of tumor characteristics. However, developing such systems requires addressing multiple technical complexities, from precise tumor delineation to accurate grading.

In this project, we trained a hybrid model for brain tumor detection and classification from MRI scans using BraTS dataset. Our approach combines the strengths of deep learning-based segmentation with traditional machine learning classification. Specifically, we utilize a (U-Net) architecture to segment tumor regions from MRI images, followed by feature extraction from these segmented areas, then processed by a Support Vector Machine (SVM) classifier to distinguish between low-grade and high-grade gliomas.

The thesis is structured as follows: We begin by introducing essential medical and technical concepts related to brain anatomy and tumor classification. We then explore the theoretical foundations of artificial intelligence, machine learning, and deep learning. Next, we review the state-of-the-art approaches in brain tumor detection. Finally, we present our methodology, results, and a demonstration of our system's practical application.

Chapter 1

Medical and Technical Concepts

1.1 Introduction

This chapter provides essential background information on the clinical and technological context of the thesis. We begin by describing the brain and its tissues from both macroscopic and microscopic perspectives. We then discuss brain tumors, which are the primary focus of this research. Next, we introduce the different types of medical imaging modalities and explain the importance of segmentation tasks in neuro-oncology. Finally, we delve deeper into the principles and components of Magnetic Resonance Imaging (MRI), which is the primary imaging modality used in this thesis.

1.2 The Microscopic Description of the Brain

The human brain is an irregular, ovoid organ with a large anteroposterior axis. Its average volume is approximately 1100 cm^3 in women and 1400 cm^3 in men, and it weighs between 1400 g and 1800 g. It occupies the cranial cavity but does not contact the bone directly, as it is suspended in cerebrospinal fluid inside a fluid chamber [10].

The brain comprises four main regions: the cerebrum, cerebellum, brainstem, and diencephalon (Figure 1.1).

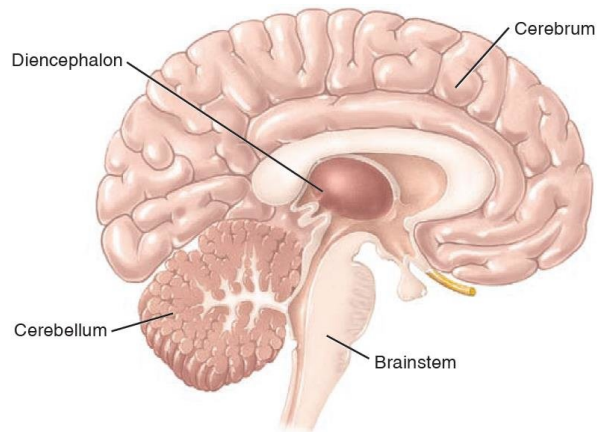


Figure 1.1: Brain main parts: cerebrum, cerebellum, brainstem, and diencephalon [1].

Cerebrum

The cerebrum is the largest part of the brain, representing about 83% of its total volume. It is divided into right and left hemispheres connected by the corpus callosum. Each hemisphere controls the contralateral side of the body.

Cerebellum

The cerebellum lies below the cerebrum and accounts for about 11% of brain volume. It coordinates reflexes, movement, balance, and posture.

Brainstem

The brainstem connects the cerebrum and cerebellum to the spinal cord and controls vital functions such as eye movements, breathing, blood pressure, and heart rate.

Diencephalon

Surrounded by the cerebral hemispheres, the diencephalon coordinates motor functions, maintains consciousness, regulates autonomic functions (eating, thirst, temperature, circadian rhythm) and interacts with both brain and cerebellum [11].

1.3 Brain Tissue

The brain's anatomical structures can be divided into hemispheres and lobes, but in medical imaging, voxels are typically classified into three main tissue types: gray matter, white matter,

and cerebrospinal fluid (CSF) [12].

Gray Matter

Gray matter contains neuronal cell bodies (soma), axon tracts, glial cells, capillary blood vessels, and neuropil (dendrites, unmyelinated axons, glia) [13].

White Matter

White matter consists primarily of myelinated axons (tracts), oligodendrocytes, and astrocytes, forming the brain's long-range connections [13].

Cerebrospinal Fluid

Cerebrospinal fluid (CSF) cushions the brain and spinal cord, removes metabolic waste, and maintains proper central nervous system function [14].

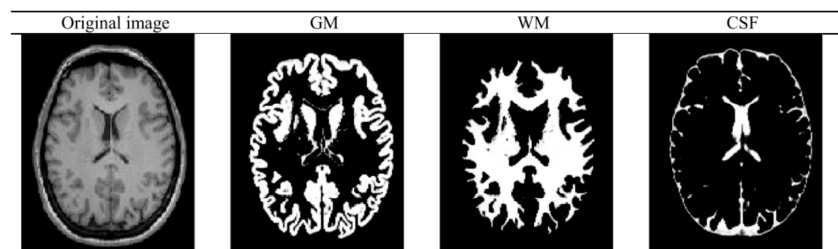


Figure 1.2: Segmentation of a brain MRI into gray matter (GM), white matter (WM), and CSF by Statistical Parametric Mapping (SPM) [2].

1.4 Classification of Brain Tumors

Brain tumors can be categorized by their biological behavior and histology. The World Health Organization (WHO) broadly classifies them as benign, premalignant, or malignant based on growth rate, invasiveness, and cellular atypia [15].

1.4.1 Benign Tumors

Benign tumors grow slowly and do not invade surrounding brain tissue. Histologically, their cells resemble normal counterparts and exhibit low mitotic activity. Common examples

include meningiomas and pituitary adenomas, which often present with well-circumscribed margins and have favorable prognoses following surgical resection [15].

1.4.2 Premalignant Tumors

Premalignant lesions (WHO Grade I–II) display atypical cellular features and proliferative potential higher than benign lesions, yet lack overt invasive behavior. These tumors may progress to higher grades over time, and thus require close monitoring and, in some cases, adjuvant therapy.

1.4.3 Malignant Tumors

Malignant tumors (WHO Grade III–IV) are characterized by rapid growth, high mitotic index, and the ability to infiltrate adjacent neural structures. They often recur despite multimodal treatment (surgery, radiotherapy, chemotherapy) and carry poor overall survival [15].

1.5 Common Intracranial Tumor Types

The three most frequent primary brain tumors in adults are [16]:

- **Meningioma.** Originating from the arachnoidal cap cells of the meninges, meningiomas are typically benign (WHO Grade I), slow-growing, and extra-axial. They often cause symptoms by mass effect rather than infiltration.
- **Pituitary Adenoma.** Arising in the anterior pituitary gland, these adenomas are usually benign but can lead to endocrine dysfunction and visual disturbances due to suprasellar extension.
- **Glioma.** Gliomas arise from glial cells and represent the majority of malignant primary CNS tumors. They are graded by WHO as:
 - *Low-Grade Glioma (LGG, Grades I–II).* Slow-growing, with diffuse infiltration but relatively favorable prognosis.
 - *High-Grade Glioma (HGG, Grades III–IV).* Aggressive, with high proliferative index and poor survival; includes anaplastic astrocytoma (Grade III) and glioblastoma

multiforme (Grade IV).

Accurate grading of gliomas (LGG vs. HGG) is critical for treatment planning and prognosis, and motivates the need for precise segmentation and classification pipelines.

1.6 Signs and Symptoms Associated with Brain Tumors

Brain tumors are the most common cause of death among all people and childhood cancers according to the Surveillance, Epidemiology, and End Results Program. Signs and symptoms depend on a variety of factors, including location of the tumor, age of the person, and rate of tumor growth. Patients with brain tumors develop focal (e.g., motor deficits, seizures, ocular impairments, urinary incontinence, and speech impediments) and/or generalized neurological symptoms and signs (e.g., headache, nausea, vomiting, dizziness, sleep-wake disturbances, and mental status abnormalities) [17].

1.7 Diagnosis of Brain Tumors

The diagnosis of brain tumors is a complex process that requires a combination of clinical evaluation, imaging studies, and sometimes invasive procedures. The following sections outline the key components of this diagnostic process.

1.7.1 Physical Examination

One of the basics of this examination is that the doctor diagnoses the condition of the patient who is under suspicion of a brain tumor, where the doctor studies his condition by interrogating the patient to verify whether there are clinical signs that in turn lead the doctor to do a clinical examination that focuses on functions in which the brain intervenes, such as memory, emotions, understanding the language, feel of touch. By testing these functions, the peripheral symptoms can be detected, and therefore the affected area of the brain.

1.7.2 Complementary Examination

In most cases, the patient's condition requires the doctor to perform various tests, including a lumbar puncture. This is a test in which a sample of the spinal brain fluid is taken by sticking a

needle into the lower stem of the spine, with the patient lying on the left side, a needle inserted into the L3 to L4 or L4 to L5. Afterwards, the sample is analyzed to find any cancer cells present for the tumor.

1.7.3 Brain Biopsy

Biopsy is a risky process that can cause bleeding while the surgeon is operating under the patient's total anesthesia, as well as a potential transmission of an infection, whether blood infection or other infection. The goal of this process is to search for cancer and determine its nature by surgically removing a sample of tissues taken from the tumor for closer examination to ascertain the nature of the tissues that are unknown.

1.7.4 Medical Imaging

This examination is based on imaging techniques such as MRI and computed tomography (CT) scanner or CT scan. MRI was adopted for its unique feature of having detailed, and also it is good technique for knowing the brain tumor in human body, where in the following we will present the general front and characteristics of it [18].

1.8 Medical Imaging in Brain Tumor Diagnosis

Magnetic Resonance Imaging (MRI) has emerged as the gold standard for brain tumor diagnosis due to its superior soft tissue contrast, high spatial resolution, and non-invasive nature. Unlike other imaging modalities such as CT scans, MRI provides detailed structural information without exposing patients to ionizing radiation, making it particularly valuable for serial monitoring and treatment planning [19].

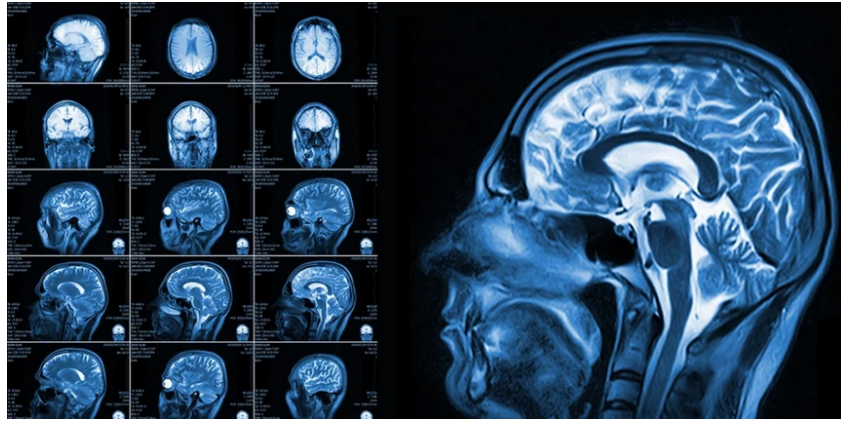


Figure 1.3: Example of brain MRI image. [3]

The multimodal nature of MRI is especially useful in brain tumor assessment, with each sequence highlighting different aspects of the tumor:

- **T1-weighted (T1):** Provides excellent anatomical detail and clearly delineates boundaries between gray and white matter. Tumors typically appear hypointense (darker) compared to surrounding tissue.
- **T1 with contrast enhancement (T1ce):** After gadolinium administration, areas with disrupted blood-brain barrier (characteristic of high-grade tumors) enhance, appearing hyperintense and revealing the active tumor core.
- **T2-weighted (T2):** Highlights areas with increased water content, making it valuable for identifying edema and infiltrative tumor components. Tumors and surrounding edema appear hyperintense.
- **Fluid-Attenuated Inversion Recovery (FLAIR):** Suppresses cerebrospinal fluid signals, enhancing the visibility of periventricular lesions and edema associated with tumors.

Traditionally, neuroradiologists diagnose brain tumors by visually inspecting these multiple MRI sequences, mentally integrating information across modalities to determine tumor boundaries, assess grade, and identify critical structures [20]. This process is inherently subjective, time-consuming, and susceptible to inter-observer variability, with studies reporting considerable disagreement even among experienced radiologists. These limitations have driven significant interest in developing computational approaches for automated and semi-automated

tumor analysis.

1.9 Conclusion

This chapter introduced the fundamental concepts of brain anatomy, tumor classification, and magnetic resonance imaging (MRI) modalities. We discussed the importance of accurate segmentation and classification of brain tumors and the traditional approach of manual diagnosis by radiologists. We also outlined the limitations and challenges of this approach, highlighting the need for computational methods to improve the accuracy and efficiency of brain tumor diagnosis.

Chapter 2

Deep Learning and Machine Learning

2.1 Introduction

Artificial intelligence (AI) has become indispensable in medical imaging, offering tools that can assist—and in some cases outperform—radiologists in detecting and characterizing pathologies. In the context of brain tumors, AI-driven methods enable rapid and accurate identification of tumor boundaries and grading, directly impacting treatment planning and patient outcomes.

In this chapter,

2.2 What is Artificial Intelligence?

Artificial Intelligence (AI) is a multidisciplinary field focused on developing machines and computer programs capable of performing tasks that typically require human intelligence, such as visual perception, reasoning, decision making, and language understanding. According to [21], AI is defined as:

"the science and engineering of creating intelligent machines, particularly intelligent computer programs that can perform tasks requiring human intelligence, such as visual perception, decision making, and language translation."

In other words, AI includes both the study of human cognition—how people perceive,

learn, reason, and decide—and the development of algorithms and systems that can perform tasks requiring "intelligence," such as visual recognition or decision making. While some AI techniques draw inspiration from biological processes (e.g. neural networks), the field also embraces purely mathematical and statistical methods.

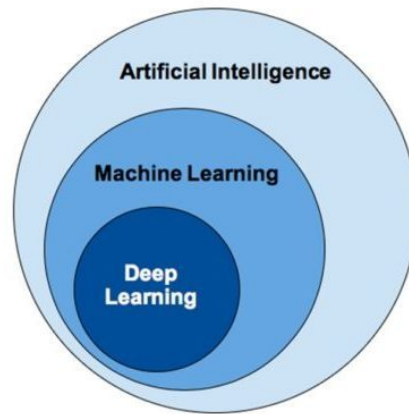


Figure 2.1: Differences between AI, machine learning, and deep learning. [4]

2.3 Machine Learning

Machine learning (ML) has emerged as a crucial area of study for organizations aiming to harness data resources and gain deeper insights into their operations. Unlike traditional programming methods, where explicit instructions are coded, machine learning enables systems to learn directly from data. In the medical imaging field, ML techniques offer powerful ways to analyze complex MRI data, supporting more accurate and efficient diagnostic processes. However, machine learning is a complex process that involves using diverse algorithms to iteratively learn from data, refine data representations, and make predictions. By feeding training data into these algorithms, increasingly accurate models can be developed. These machine learning models represent the knowledge acquired by algorithms during the training phase [22].

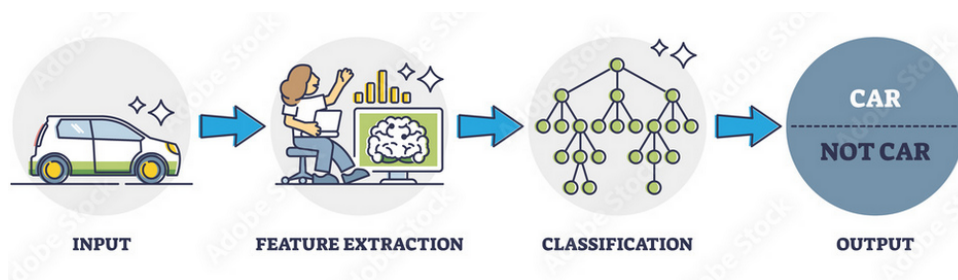


Figure 2.2: Illustration of the Machine Learning Process [5]

2.3.1 Why Machine Learning?

Machine learning offers several compelling advantages that have driven its adoption in medical imaging and other fields:

- **Pattern Recognition in Complex Data:** Machine learning excels at discovering patterns in high-dimensional data that may be imperceptible to human observers. For medical imaging, this means identifying subtle tissue abnormalities or correlations that might otherwise be missed.
- **Automation of Repetitive Tasks:** ML algorithms can automate time-consuming aspects of image analysis, freeing radiologists to focus on interpretation and clinical decision-making rather than routine measurements or screenings.
- **Quantitative Assessment:** Unlike qualitative human evaluations that may vary between observers, machine learning provides consistent, quantitative measurements of disease characteristics, potentially reducing inter-observer variability.
- **Integration of Multimodal Data:** Modern ML methods can combine information from multiple imaging modalities (MRI, CT, PET) along with clinical data to provide more comprehensive analysis than would be possible with any single data source.
- **Predictive Capabilities:** Beyond current state assessment, machine learning can predict disease progression or treatment response based on patterns learned from large datasets of prior patients.
- **Personalized Medicine:** ML algorithms can identify subgroups of patients with similar characteristics or disease presentations, enabling more tailored treatment approaches.
- **Continuous Learning:** Machine learning systems can be designed to improve over time as they process more data, unlike traditional rule-based systems that remain static unless manually updated.
- **Cost-Effectiveness:** By improving diagnostic accuracy and efficiency, machine learning can reduce unnecessary tests, treatments, and hospitalizations, potentially lowering healthcare costs.

2.3.2 Machine Learning Application Examples

Machine learning has been successfully applied across numerous domains, with far-reaching impacts in areas such as computer vision, natural language processing, and recommender systems:

- **Tumor Detection and Classification:** ML algorithms can detect and classify brain tumors, lung nodules, and other cancerous lesions from imaging data [23].
- **Disease Progression Monitoring:** Tracking changes in disease markers over time, such as multiple sclerosis lesion load or Alzheimer's-related brain atrophy [24].
- **Radiomics:** Extracting quantitative features from medical images to improve diagnostic and prognostic accuracy [25].
- **Resource Allocation:** Predicting hospital readmissions or length of stay to optimize resource allocation [26].
- **Algorithmic Trading:** Making trading decisions based on market data analysis [27].
- **Recommendation Systems:** Suggesting products or content based on user preferences and behavior [28].
- **Churn Prediction:** Identifying customers likely to discontinue services [29].
- **Supply Chain Optimization:** Predicting demand and optimizing inventory management [30].
- **Resource Management:** Optimizing water and energy resource allocation [31].

2.3.3 Different Techniques and Algorithms in Machine Learning

Machine learning encompasses a diverse array of techniques and algorithms, each with unique strengths for specific types of problems, we mention some of them:

Classification Algorithms:

- **Support Vector Machines (SVMs):** Algorithms that find the optimal hyperplane to separate classes in high-dimensional space [32].

- **Random Forests:** Ensemble learning methods that construct multiple decision trees and output the class that is the mode of the classes of individual trees [33].
- **Naive Bayes:** Probabilistic classifiers based on applying Bayes' theorem with strong independence assumptions [34].
- **k-Nearest Neighbors (k-NN):** Instance-based learning where an object is classified by a majority vote of its neighbors [35].

Regression Algorithms:

- **Linear Regression:** Modeling the relationship between a dependent variable and independent variables using a linear approach [36].
- **Lasso Regression:** Linear regression with L1 regularization that can perform feature selection [37].
- **Gaussian Process Regression:** A non-parametric approach using Gaussian processes for modeling [38].

Clustering Algorithms:

- **K-Means:** Partitioning observations into k clusters based on the nearest mean [39].
- **Hierarchical Clustering:** Building a hierarchy of clusters either through agglomerative or divisive approaches [40].

2.3.4 Machine Learning approaches

Machine learning algorithms can be categorized into three main categories: supervised learning, unsupervised learning, and reinforcement learning. In the following sections, we will explore each of these categories in more detail, highlighting their strengths and weaknesses, and providing examples of how they are used in medical imaging analysis.

2.3.4.1 Supervised Learning

In supervised learning, the algorithm learns from labeled training data, where each data point is associated with a corresponding label or target value as depicted in Figure 2.3. Ex-

amples of supervised learning algorithms include linear regression , decision trees , random forests , support vector machines.

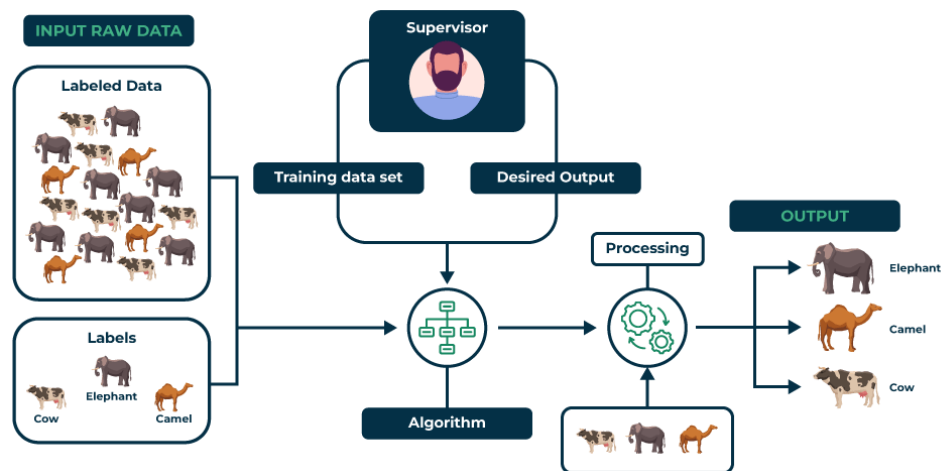


Figure 2.3: Illustration of the Supervised learning process [6]

2.3.4.2 Unsupervised Learning

Unsupervised learning deals with unlabeled data, where the algorithm learns to find patterns or structure in the data without any specific guidance. Such as k-means and hierarchical clustering, and dimensionality reduction techniques, such as principal component analysis and t-distributed stochastic neighbor embedding, Figure 2.4

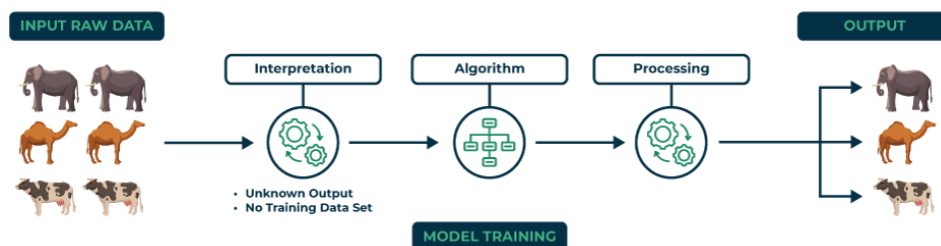


Figure 2.4: Illustration of the Unsupervised learning process [6]

2.3.4.3 Reinforcement Learning

Reinforcement learning is a type of machine learning where an agent learns to make decisions by interacting with an environment. The agent receives feedback in the form of rewards or penalties based on its actions, allowing it to learn optimal strategies over time. This approach is often used in robotics, game playing, and autonomous systems. Figure 2.5 illustrates the reinforcement learning process.

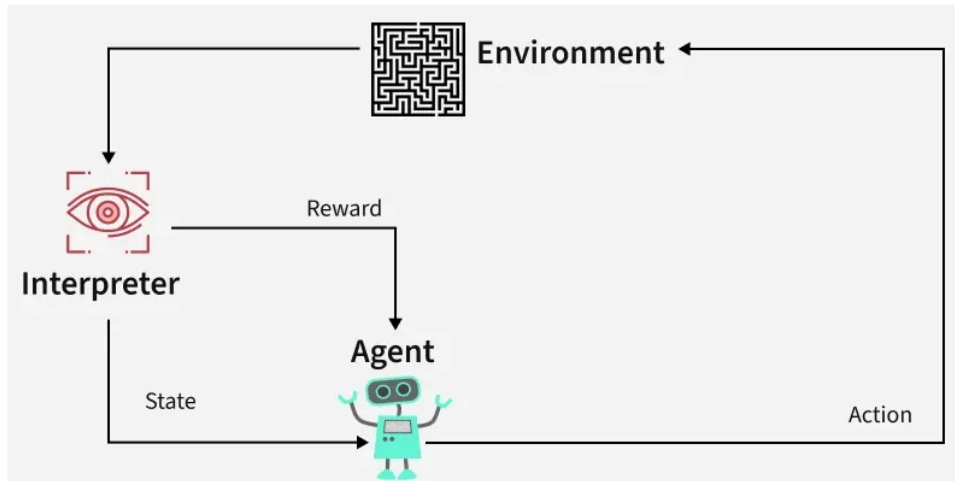


Figure 2.5: Illustration of the Reinforcement learning process [6]

2.4 Deep Learning

Deep learning has emerged as a powerful approach for modeling complex data through architectures that incorporate non-linear transformations. Neural networks, including deep neural networks, serve as the fundamental components of deep learning. These techniques have achieved remarkable progress in various domains such as sound and image processing, enabling tasks like facial recognition, speech recognition, computer vision, language processing, and text classification. The potential applications of deep learning are vast and continue to expand.

Different types of neural network architectures, such as multilayer perceptrons, Convolutional Neural Networks (CNNs), and recurrent neural networks, cater to specific data types and tasks. These architectures are characterized by deep layers organized in a cascading manner.

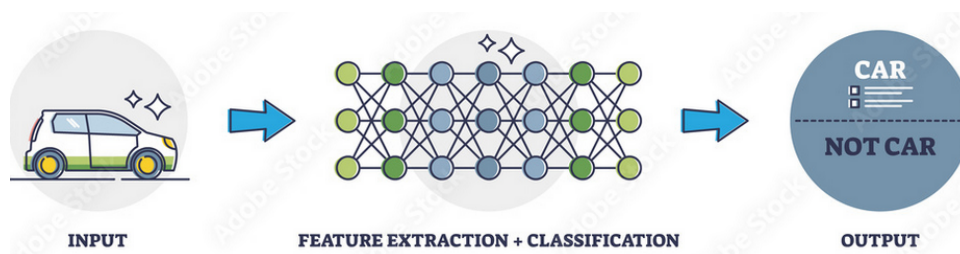


Figure 2.6: Illustration of the Deep Learning Process. [5]

2.4.1 Why Deep Learning?

Deep learning offers several distinct advantages that have fueled its adoption across numerous domains, particularly in medical imaging:

- **Automatic Feature Extraction:** Unlike traditional machine learning that relies on hand-crafted features, deep learning automatically discovers relevant features from raw data, eliminating the need for domain-specific expertise in feature engineering [41].
- **Hierarchical Feature Learning:** Deep networks learn representations at multiple levels of abstraction. Lower layers capture basic patterns (e.g., edges in images), while higher layers combine these to represent complex concepts (e.g., textures, objects, or tumor characteristics) [41].
- **Scalability with Data:** Deep learning models continue to improve as more data becomes available, unlike many traditional algorithms that plateau in performance. This is particularly relevant in medical imaging as dataset sizes continue to grow [41].
- **Transfer Learning:** Knowledge gained from one task can be transferred to another, reducing the need for large amounts of labeled data for each new application—crucial in medical domains where annotated data is often scarce [42].
- **End-to-End Learning:** Deep learning can learn directly from raw input to desired output, eliminating intermediate processing steps that might introduce biases or errors [43].
- **Handling Unstructured Data:** Medical images, natural language reports, and other unstructured data that constitute most healthcare data are particularly well-suited for deep learning approaches [41].

2.4.2 Deep Learning Application Examples

Deep learning has revolutionized numerous fields with successful applications across diverse domains:

- Retinal disease detection from optical coherence tomography
- Lung cancer detection and classification from CT scans

- Skin lesion classification for melanoma detection
- Breast cancer detection in mammography
- Object detection and recognition in images and video
- Facial recognition and emotion detection
- Sentiment analysis in social media and customer feedback
- Text summarization and content generation
- Speech recognition and transcription

These few mentioned examples illustrate deep learning's versatility and transformative impact across domains.

2.4.3 Different Architectures of Deep Learning

Deep learning encompasses a variety of architectural paradigms, each designed to address specific types of problems:

Feedforward Neural Networks (FNNs): The most basic architecture where information flows only in one direction, from input to output. Multilayer Perceptrons (MLPs) are a common type of FNN with multiple hidden layers, suitable for tabular data and basic pattern recognition tasks.

Convolutional Neural Networks (CNNs): Specialized for processing grid-like data such as images. CNNs employ convolutional layers that apply filters across the input, capturing spatial hierarchies and patterns. Notable CNN architectures include:

- **AlexNet:** Pioneering architecture that demonstrated the power of deep learning in computer vision [44]
- **VGGNet:** Featured uniform architecture with small filters [45]
- **ResNet:** Introduced residual connections to train very deep networks effectively [46]
- **Inception/GoogLeNet:** Employed multi-scale processing through parallel convolutional filters [47]

- **DenseNet**: Connected each layer to every other layer in a feed-forward fashion [48]
- **U-Net**: Specialized for biomedical image segmentation with a contracting path and an expansive path [49]

Recurrent Neural Networks (RNNs): Designed for sequential data by maintaining internal memory states. Variants include:

- **Long Short-Term Memory (LSTM)**: Addresses the vanishing gradient problem with specialized memory cells [50]
- **Gated Recurrent Units (GRU)**: Simplified version of LSTM with fewer parameters [51]
- **Bidirectional RNNs**: Process sequences in both forward and backward directions

Transformer Networks: Introduced in the paper "Attention Is All You Need" [52], transformers rely on self-attention mechanisms rather than recurrence or convolution. They have revolutionized NLP through models like BERT, GPT, and T5, and are increasingly applied to computer vision tasks.

Generative Models:

- **Generative Adversarial Networks (GANs)**: Consist of generator and discriminator networks trained simultaneously in a minimax game [53]
- **Variational Autoencoders (VAEs)**: Encode inputs to a latent space distribution and decode samples from this distribution [54]
- **Diffusion Models**: Generate data by gradually removing noise from a signal [55]

Hybrid Architectures: Many modern deep learning solutions combine elements from different architectural paradigms to leverage their respective strengths. For example, CNN-LSTM networks for video analysis or attention-augmented CNNs for improved image recognition.

2.4.4 Convolutional Neural Networks (CNNs)

A convolutional neural network (CNN) is a type of neural network with a topology similar to a grid, inspired by the human brain. It is commonly used for image processing tasks, as well as natural language processing.

A CNN consists of two main parts. The input is an image, represented as a 2D matrix of pixels for grayscale images and a 3D matrix of pixels for color images (Red, Green, Blue).

The first part of a CNN is the convolutional layer, which acts as a feature extractor. The image is passed through a series of filters, or convolution kernels, to generate new images called feature maps. Some intermediate filters reduce the image resolution. Finally, the feature maps are concatenated to form a vector of features, known as the CNN code.

The output of the convolutional layer, the CNN code, is the input to the second part of the network. The main role of this part is to combine the features of the CNN code to classify the image. The output is a final layer with one neuron per category.

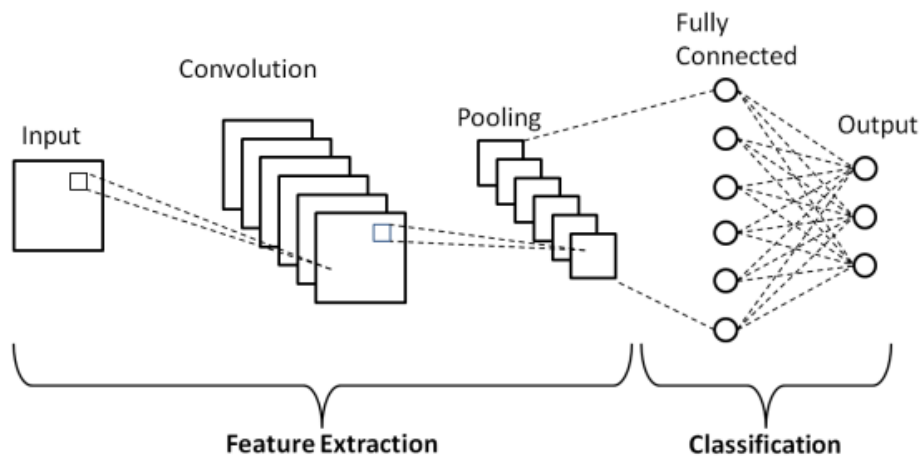


Figure 2.7: Convolutional Neural Network Architecture [7]

2.4.4.1 Convolutional Layer

The convolutional layer is the most important layer and usually the first layer in a CNN. It takes an image and a filter as input and applies the convolution operation to produce a new image, called the activation map or feature map.

The activation map values are calculated using the following formula:

$$G[m,n] = (f * h)[m,n] \quad (2.1)$$

where

- f is the input image,

- h is the convolution filter,
- m, n are the spatial indices over which the convolution is computed.

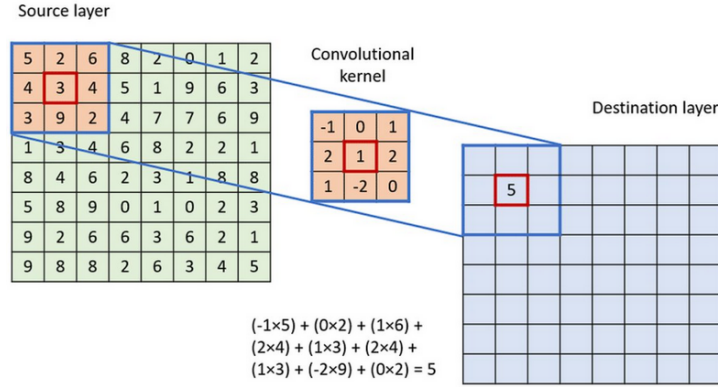


Figure 2.8: Convolution Layer in a Convolutional Neural Network [8]

2.4.4.2 Correction Layer (ReLU)

The Correction Layer, typically implemented using the Rectified Linear Unit (ReLU), is an activation function applied after each convolution operation to enhance processing efficiency. It replaces all negative pixel values with zero, introducing non-linearity into the network while maintaining computational simplicity. The ReLU function is defined as:

$$f(x) = \max(0, x) \quad (2.2)$$

Several other activation functions exist, such as the sigmoid function, the hyperbolic tangent function (tanh), and the hyperbolic saturating tangent function. However, ReLU is often preferred in deep learning models because it enables faster convergence and better performance compared to these alternatives.

2.4.4.3 Pooling Layers

Pooling layers are utilized to reduce the spatial dimensions of feature maps while preserving the most important information and features. This helps decrease computational complexity and mitigate overfitting. There are several types of pooling operations:

- **Max Pooling:** It selects the maximum value from each patch of the feature map. Typically, a 2×2 patch is used. Max pooling is the most commonly used pooling method.

- **Min Pooling:** The inverse of max pooling; it selects the minimum value from each patch of the feature map.
- **Average Pooling:** It computes the average of all the values within each patch of the feature map by summing the values and dividing by the number of elements.
- **Sum Pooling:** It computes the sum of all elements within each patch of the feature map.
- **Flattening:** After the pooling operations, the resulting feature maps are flattened into a single one-dimensional vector to prepare for fully connected (dense) layers.

2.4.4.4 Fully Connected Layer

after the convolution and pooling layers, the high-level reasoning in the neural network is done in fully connected layers. The output of flattening is the input of FC layers which are the same as artificial neural networks and carry out the same mathematical operations. The last fully-connected layer uses an activation function such as sigmoid or softmax to get probabilities of the outputs.

2.5 Conclusion

In this chapter, we established the core concepts and distinctions between AI, machine learning, and deep learning, reviewed key algorithms and architectures—from SVMs and decision forests to CNNs, transformers, and U-Nets—and illustrated how these methods enable robust pattern recognition, automated analysis, and end-to-end learning on complex medical imaging data; this theoretical foundation directly supports our subsequent work on brain tumor segmentation and classification, where we will detail data preprocessing, the U-Net implementation, and model evaluation against clinical standards.

Chapter 3

State of the art on Brain Tumor Detection methods

3.1 Introduction

This chapter reviews the significant literature connected to this study, which aims to establish a conceptual information system framework for medical imaging employing MRI brain tumor pictures. The review focuses on the use of accessible current electronic scanners, computer-based methodologies, and their application to enhance the MRI brain tumor tissue analysis with a comparable accuracy to manual analysis methodology.

3.2 Literature Review

3.2.1 Contemporary Methods for Tissue Analysis

The routine examination of tissues is essential for understanding disease progression and diagnosis. With the increasing availability of medical imaging, it provides an unprecedented opportunity to non-invasively visualize tissue samples and diagnose various medical conditions. In order to make this diagnosis, there are three possible ways to perform this examination in the laboratory, including:

3.2.1.1 Traditional Microscopic Analysis

Histopathological examination remains a cornerstone in disease diagnosis, relying on the meticulous preparation and analysis of tissue specimens. The standard workflow encompasses several critical steps:

1. **Fixation:** Immediately after collection, tissue samples are immersed in a fixative, typically 10% neutral buffered formalin, to preserve cellular structures and prevent degradation [56].
2. **Processing and Embedding:** Fixed tissues undergo dehydration through a series of alcohol baths, clearing with xylene, and infiltration with paraffin wax. This process solidifies the tissue, facilitating thin sectioning [57].
3. **Sectioning:** Using a microtome, thin sections (commonly 3–5 μm) are sliced from the paraffin-embedded tissue blocks and mounted onto glass slides [56].
4. **Staining:** Sections are stained, most commonly with hematoxylin and eosin (H&E), to differentiate cellular components and enhance contrast for microscopic evaluation [58].

Pathologists examine these slides under varying magnifications (e.g., 10 \times , 20 \times , 40 \times , 100 \times) to assess tissue architecture and identify pathological changes [59].

3.2.1.2 Medical Imaging Modalities for Tissue Analysis

Medical imaging plays a pivotal role in the non-invasive diagnosis and evaluation of various medical conditions, including brain tumors. The primary imaging modalities include ultrasound (US), computed tomography (CT), and magnetic resonance imaging (MRI), each with distinct advantages and limitations.

Ultrasound: Ultrasound imaging utilizes high-frequency sound waves to produce real-time images of internal body structures. It is widely used due to its safety, cost-effectiveness, and portability. However, ultrasound has limitations in imaging structures that are deep within the body or surrounded by bone, such as the brain, making it less suitable for detecting small or deep-seated tumors [60].

Computed Tomography (CT): CT scans employ ionizing radiation to generate cross-

sectional images of the body. They are particularly effective in visualizing bone structures and detecting acute conditions like hemorrhages. CT scans are faster and more accessible than MRI, making them valuable in emergency settings. However, their ability to differentiate soft tissues is inferior to that of MRI, and the use of ionizing radiation poses potential risks with repeated exposure [61].

Magnetic Resonance Imaging (MRI): MRI uses strong magnetic fields and radiofrequency pulses to produce detailed images of soft tissues without ionizing radiation. It offers superior contrast resolution, making it the preferred modality for brain imaging and the detection of tumors, strokes, and other neurological conditions. MRI's ability to distinguish between different soft tissues surpasses that of CT, providing more precise information for diagnosis and treatment planning [62].

3.2.1.3 Computer-Aided Diagnosis Using Digitized Histopathology Slides

Traditional manual examination of histopathological slides is time-consuming, subject to inter-observer variability, and may lead to inconsistent diagnostic outcomes. To address these challenges, computer-aided diagnosis (CAD) systems have been developed to assist pathologists by providing quantitative analyses of digitized histopathology images.

CAD systems utilize advanced image processing and machine learning techniques to analyze features such as color, texture, and morphological patterns within tissue samples. For instance, Elazab et al. developed a CAD system that grades brain tumors by extracting color and texture features from histopathology images, achieving significant accuracy in tumor classification [63].

Furthermore, automated classification methods have been applied to whole-slide digital pathology images. Barker et al. proposed an approach that segments whole-slide images into representative tiles and classifies brain tumors using machine learning algorithms, demonstrating high diagnostic accuracy [64].

3.2.2 Image processing techniques

3.2.2.1 Image Pre-processing

The medical images processed contain a great deal of information as they are usually noisy due to unwanted pixels. It is always necessary to preprocess as a first step in most current image analysis techniques to analyze the image of the brain tumor where pre-processing aims to improve:

1. **Noise removal:** Removing impulse noise from images is one of the most important concerns in digital image processing, where noise must be removed in a way that preserves the important information of the image. A variety of techniques are used to eliminate and reduce noise in images, including a Gaussian filter, which is used to remove details and noise. It provides positive and enhanced results for noisy images.
2. **Enhance contrast:** It is defined as the manipulation and redistributing the image pixels in a linear or non-linear fashion to improve the separation of obscured structural variations in pixel intensity into a more visually differentiable structural distribution. However, there is no universal theory for enhance contrast approach. Digitized images acquired from MRI are typically grayscale images. It is hard to deal with the intensity of a grayscale image straightway [65]. The processing of contrast enhancement histograms is one of the most widely used approaches. The processing of histogram includes equalization (An approach that extends the intensity range and improves image contrast.) and normalization (An approach for modifying the series of pixel intensity values according to relative frequencies).

3.2.2.2 Segmentation

Segmentation is the most important part in image processing. Fence off an entire image into several parts which is something more meaningful and easier for further process. These several parts that are rejoined will cover the entire image. Segmentation may also depend on various features that are contained in the image. It may be either color or texture. Before denoising an image, it is segmented to recover the original image. The main motto of segmentation is to reduce the information for easy analysis. Segmentation is also useful in Image Analysis and Image Compression [66].

3.2.2.3 classification

Although there are many techniques used to identify and classify each depending on the characteristics they target for detection, for images of MRI brain tumor, there are three basic characteristics (shape, size, and color) required for tumor detection. In most cases, the svm algorithm is used, but more recently, the Convolutional Neural Network approach is also widely used in medical image processing.

3.2.2.4 Detection

Image detection is a technique that analyzes the picture and finds items inside it, medical image detection refers to the process of recognizing medical-related objects that are included within an image. This assists in establishing the precise placement of multiple tissues as well as the direction of those tissues.

3.3 Related Work

In this section, we review key approaches to brain tumor segmentation and classification that motivated our work. We focus on some representative studies, highlighting their main techniques and results, and then summarize them in Table 3.1.

3.3.1 Brain Tumor Segmentation and Grading of Lower-Grade Glioma

Naser *et al.* [67] used a U-Net–based CNN with transfer learning from VGG16 to segment tumors in 110 T1-FLAIR cases of low-grade glioma (LGG). They then classified LGG into grade II vs III, achieving 89 % accuracy on slice-level MRI and 95 % at the patient level.

3.3.2 Wavelet Statistical Texture + RNN

Begum *et al.* [68] combined optimal wavelet statistical features with an RNN classifier. Their pipeline includes Gaussian filtering for noise removal, with feature selection, RNN classification, and tumor segmentation via a modified region growing algorithm. They reported 95 % accuracy.

3.3.3 Hybrid CNN + NADE

Hashem *et al.* [69] trained two parallel CNNs whose feature outputs are combined via a Neural Autoregressive Distribution Estimator (NADE). This joint distribution aids in tumor shape identification. Using cross-entropy loss on 3 064 T1-weighted images, they achieved 95 % accuracy.

3.3.4 Hierarchical Transfer Learning with AlexNet & GoogleNet

The framework in [70] applies skull stripping and then uses AlexNet to classify tumors into benign vs malignant, followed by GoogleNet to further distinguish malignant into glioma vs meningioma. With data augmentation (flips, rotations), they report:

- Benign vs Malignant: precision 93.75 %, recall 100 %, F1 96 %.
- Glioma vs Meningioma: precision 95 %, recall 100 %, F1 97.43 %, accuracy 97.50 %.

3.3.5 VGG Block-wise Fine-Tuning

Lee *et al.* [71] employ VGG19 with a block-wise fine-tuning strategy, dividing the network into six blocks and progressively unfreezing from the last block. Evaluated on the same 3 064 T1-weighted set, they reach 94.42 % accuracy.

Table 3.1: Summary of prior methods in brain tumor segmentation and classification

Study	Approach	Dataset	Key Results
Naser <i>et al.</i>	U-Net + VGG16 transfer learning	110 LGG (T1-FLAIR)	MRI accuracy: 89%, patient accuracy: 95%
Begum <i>et al.</i>	OGSA wavelet + RNN + MRG segmentation	BraTS2020	95% accuracy
Hashem <i>et al.</i>	Hybrid CNNs + NADE	3,064 T1-weighted images	95%
Framework	AlexNet and GoogleNet hierarchy	BraTS2020	Benign vs Mal: F1 96%; Glioma vs Men: F1 97.43%, acc 97.50%
Lee <i>et al.</i>	VGG19 block-wise fine-tuning	3,064 T1-weighted images	94.42%

3.4 Conclusion

In this chapter, we reviewed key approaches to brain tumor segmentation and classification, highlighting the most utilized machine learning and deep learning models for this purpose. We examined studies that informed our work, focusing on their methodologies and results.

Chapter 4

Contribution

4.1 Introduction

In this chapter, we present the core contributions of our work on automated brain tumor detection in MRIs. Building upon the BraTS dataset [19], our pipeline integrates a deep learning-based segmentation module with a classical machine learning classifier and culminates in a user-friendly demo application.

4.2 Proposed Framework Overview

In this section, we look at our proposed framework from a systematic perspective. The framework is designed to perform end-to-end brain tumor segmentation and classification. We will discuss the design of the final pipeline and the training workflow to achieve the desired results.

4.2.1 End-to-End Inference Pipeline

The purpose of our project is to have an end-to-end inference pipeline accepts a raw MR image as input, applies preprocessing steps, performs segmentation of the tumor region using the trained U-Net model, classifies the tumor grade via the SVM classifier, and finally outputs the original image overlaid with the segmentation mask along with the predicted grade as shown in Figure 4.1.

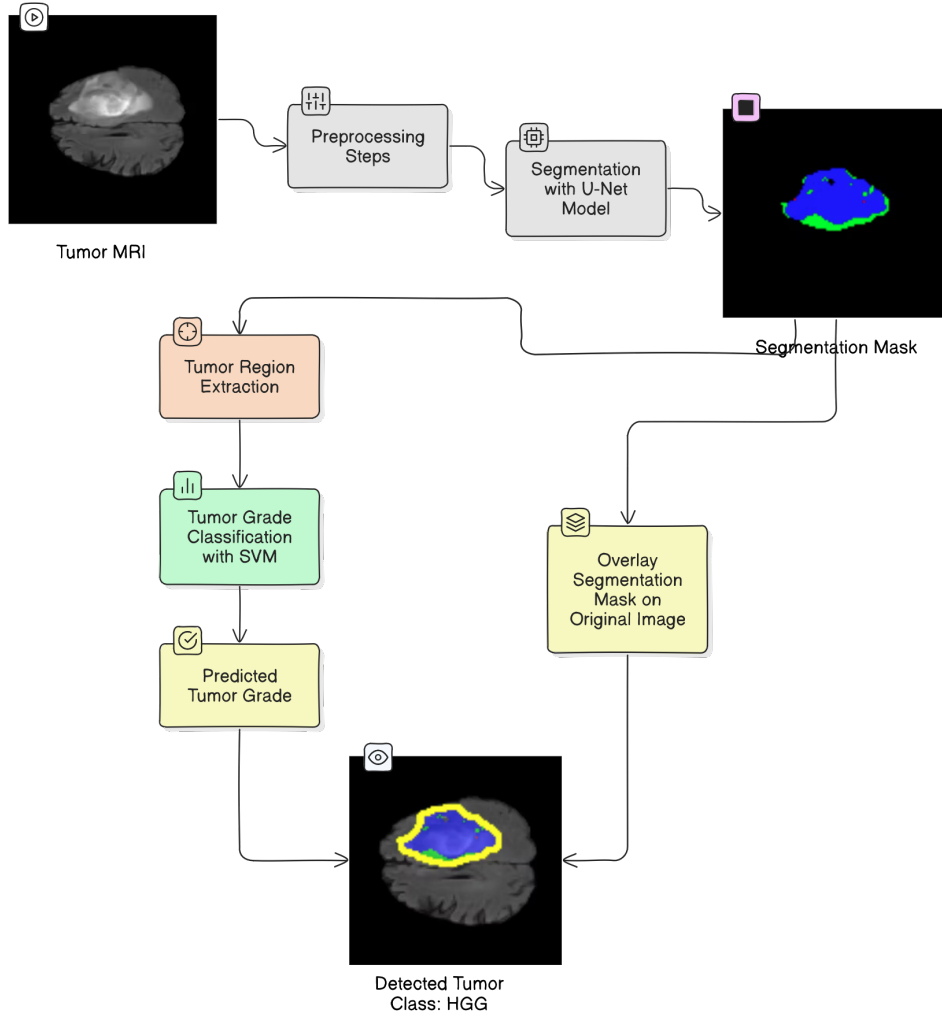


Figure 4.1: Overview of the end-to-end inference pipeline.

The selection of U-Net for tumor segmentation and Support Vector Machine (SVM) for tumor grade classification in our end-to-end inference pipeline is grounded in their proven efficacy in medical image analysis, particularly in brain tumor applications.

4.2.1.1 U-Net for Tumor Segmentation

U-Net is a convolutional neural network architecture specifically designed for biomedical image segmentation. Its encoder-decoder structure with skip connections allows for precise localization and context capture, making it highly effective for segmenting complex structures like brain tumors. Studies have demonstrated that U-Net and its variants achieve high accuracy in delineating tumor boundaries in MRI images, even with limited training data [72, 73].

Introduced by Ronneberger et al. in 2015, U-Net features a symmetric encoder-decoder

structure: the contracting path (encoder) captures image context through successive convolution and pooling operations, while the expansive path (decoder) enables precise localization via upsampling and concatenation with high-resolution features from the encoder. This architecture allows U-Net to achieve accurate segmentation even with limited annotated data by leveraging extensive data augmentation. U-Net has demonstrated superior performance in various biomedical segmentation challenges, notably outperforming previous methods in tasks such as neuronal structure segmentation in electron microscopy images and cell tracking in light microscopy [9].

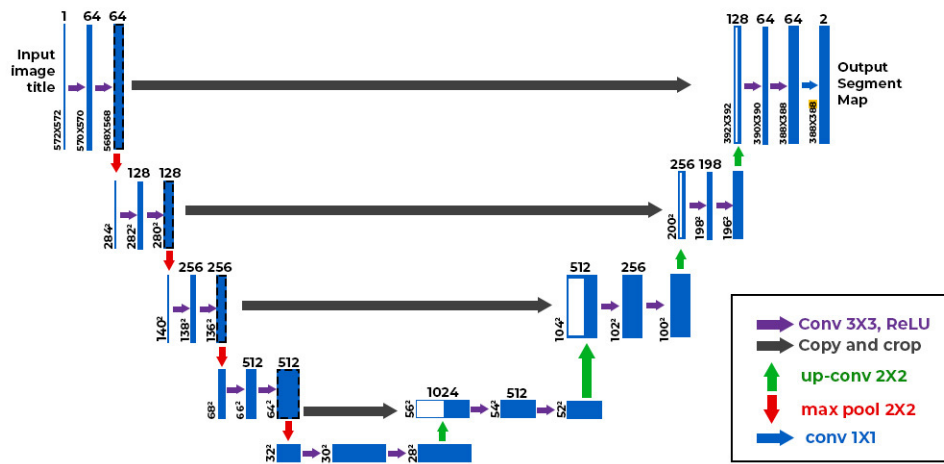


Figure 4.2: U-Net Architecture Illustrating the Encoding and Decoding Arms with Skip Connections. [9]

Key Components of a U-Net Architecture

- **Contracting Path (Encoder):**

This path is responsible for extracting contextual features from the input image. It consists of repeated blocks of two 3×3 convolutional layers (with ReLU activation), followed by a 2×2 max pooling operation for downsampling. With each downsampling step, the number of feature channels is doubled, allowing the network to capture increasingly abstract representations of the input.

- **Bottleneck:**

Located at the deepest part of the network, the bottleneck consists of convolutional layers without pooling. It serves as the bridge between the encoder and decoder, capturing the most condensed and abstract features of the input.

- **Expansive Path (Decoder):**

This path reconstructs the spatial resolution of the feature maps and enables precise localization. Each step in the decoder involves upsampling the feature map (often via transposed convolution or up-convolution), concatenating it with the corresponding feature map from the encoder (skip connection), and then applying two 3×3 convolutions (with ReLU activation). The number of feature channels is halved at each upsampling step.

- **Skip Connections:**

At each level, feature maps from the encoder are concatenated with the upsampled feature maps in the decoder. These skip connections help retain high-resolution spatial information that might otherwise be lost during downsampling, improving the accuracy of segmentation boundaries.

- **Final Output Layer:**

The last layer is typically a 1×1 convolution that maps each feature vector to the desired number of output classes, producing a pixel-wise classification map for segmentation tasks.

4.2.1.2 SVM for Tumor Grade Classification

SVM is a supervised machine learning algorithm known for its robustness in classification tasks, especially with high-dimensional data. In the context of brain tumor classification, SVM has been successfully employed to differentiate between tumor grades based on features extracted from MRI images. Its ability to handle non-linear relationships through kernel functions makes it suitable for capturing the subtle differences between low-grade and high-grade tumors [74, 64].

The theoretical foundation of SVMs is based on the Structural Risk Minimization principle, which aims to minimize an upper bound on the generalization error, offering advantages over traditional Empirical Risk Minimization approaches. Originally developed by Vapnik and colleagues in the 1990s, SVMs have become popular due to their strong empirical performance and robustness to overfitting, especially in high-dimensional spaces [75].

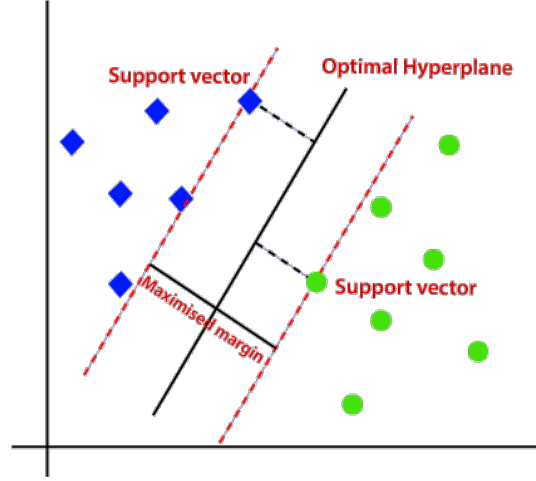


Figure 4.3: Support Vector Machine (SVM) Decision Boundary Visualization

The fundamental formula defining the decision boundary of a Support Vector Machine (SVM) is a hyperplane expressed as:

$$\mathbf{w}^\top \mathbf{x} + b = 0 \quad (4.1)$$

where \mathbf{w} is the weight vector normal to the hyperplane, \mathbf{x} is the input feature vector, and b is the bias term.

For binary classification with labels $y_i \in \{+1, -1\}$, the SVM enforces the following constraints on each training point (\mathbf{x}_i, y_i) :

$$y_i(\mathbf{w}^\top \mathbf{x}_i + b) \geq 1, \quad \forall i. \quad (4.2)$$

The margin width (the distance between the closest points of each class to the hyperplane) is given by $\frac{2}{\|\mathbf{w}\|_2}$. Maximizing this margin is therefore equivalent to minimizing $\|\mathbf{w}\|_2$, leading to the following convex optimization problem:

$$\min_{\mathbf{w}, b} \quad \frac{1}{2} \|\mathbf{w}\|_2^2, \quad (4.3)$$

$$\text{subject to} \quad y_i(\mathbf{w}^\top \mathbf{x}_i + b) \geq 1, \quad \forall i. \quad (4.4)$$

4.2.2 Models Training Workflow

In order to achieve the previous objectives, we followed a step-by-step approach. As shown in Figure 4.4, The training workflow begins with the BraTS dataset. After preprocessing and augmentation, the data is split into training, validation, and test sets. We then train the U-Net segmentation model in the other hand (separately) we train SVM classifier training, yielding two standalone models for inference that can be combined to form a hybrid model.

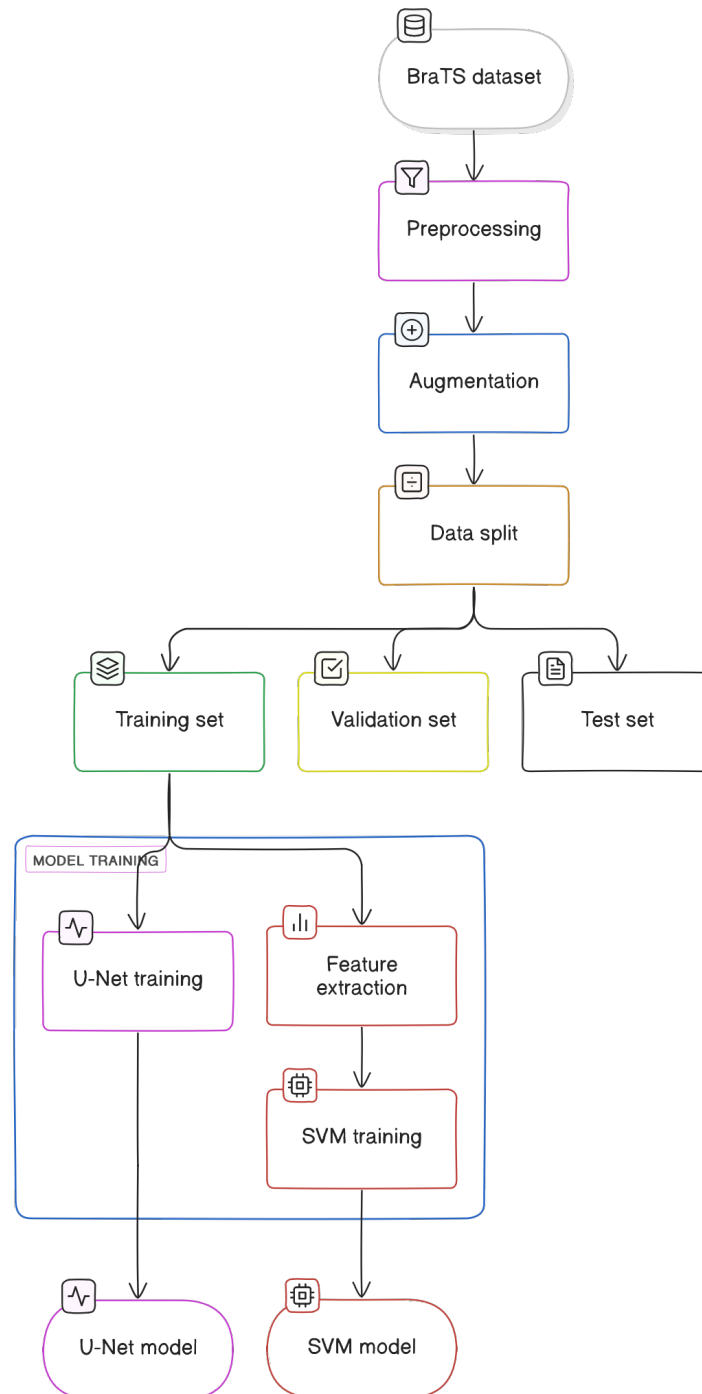


Figure 4.4: Overview of the training workflow.

4.3 Dataset and Preprocessing

In order to train our hybrid model we used the Brain Tumor Segmentation (BraTS) 2020 dataset, which is a collection of multimodal Magnetic Resonance Imaging (MRI) scans used for the segmentation of brain tumors.

4.3.1 BraTS Dataset Description

The dataset includes MRI scans (Figure 4.5) from glioma patients, providing four different MRI modalities per patient:

1. **Native (T1):** Reveals detailed anatomical structures and tissue composition, aiding in the identification of tumors, cysts, and other abnormalities.
2. **Post-contrast T1-weighted (T1ce):** Enhances tumor visibility using a gadolinium-based contrast agent, which accentuates abnormal vascularity and lesion boundaries.
3. **T2-weighted (T2):** Highlights fluid content within brain tissues, which is useful for detecting edema but can sometimes obscure lesions.
4. **T2-FLAIR (Fluid Attenuated Inversion Recovery):** Suppresses the high signal from fluids (e.g., cerebrospinal fluid), making lesions in the white matter more conspicuous.

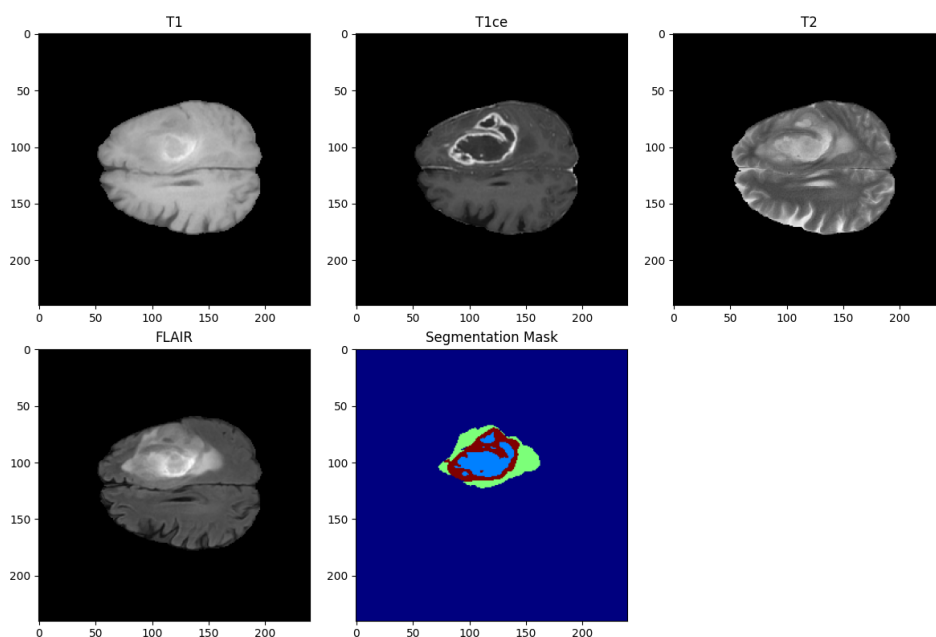


Figure 4.5: Brats modalities: T1, T1ce, T2, and T2-FLAIR.

These scans (Figure 4.5) come with expert-annotated segmentation masks that delineate the tumor into various sub-regions, such as the necrotic and non-enhancing tumor core, the peritumoral edema, and the enhancing tumor. Research has demonstrated that accurate segmentation is linked to improved prognostic assessments and treatment outcomes.

- **Class 0 (Not Tumor):** This class represents normal brain tissue or background, where no tumor tissue is present.
- **Class 1 (Non-Enhancing Tumor):** This class corresponds to the necrotic or non-enhancing core regions of the tumor. These areas typically lack contrast enhancement and may include dead or less active tumor tissue.
- **Class 2 (Edema):** This class identifies regions of peritumoral edema, which is the swelling around the tumor caused by fluid accumulation. Edema is important for understanding the extent of the tumor's impact on surrounding brain tissue.
- **Class 4 (Enhancing Tumor):** This class captures the actively enhancing parts of the tumor, visible after the administration of a contrast agent. These regions often indicate aggressive tumor tissue with increased blood flow and permeability.

To visually interpret these segmentations, we map the categorical labels to a custom colormap. In our example (Figure 4.6), we use four distinct colors to represent:

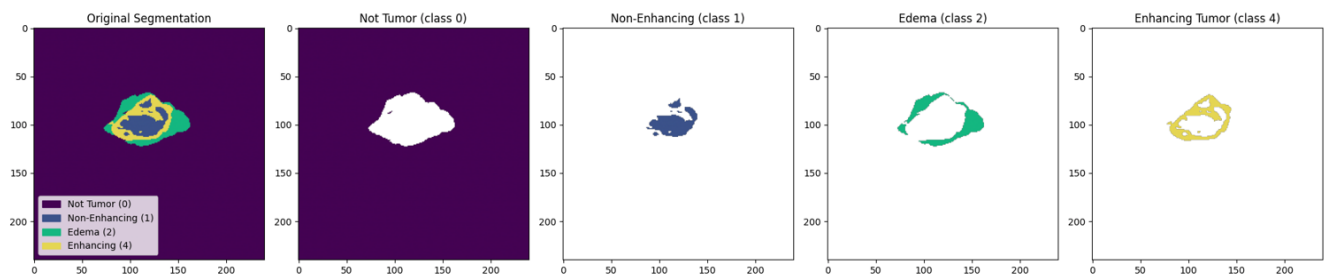


Figure 4.6: Segmentation of Tumor classes.

4.3.2 Dataset Splitting

To train and evaluate our model effectively, we need to partition our dataset into three subsets:

- **Training Set (70%):** Used to learn the model parameters.

- **Validation Set (approximately 20%):** Used for tuning hyperparameters and preventing overfitting.
- **Test Set (10%):** Used for assessing the final model’s performance on unseen data.

This split can be done randomly or in a stratified manner (to preserve the class distribution), which is especially useful when dealing with imbalanced datasets. Properly splitting the dataset is crucial for building a robust model that generalizes well to new data.

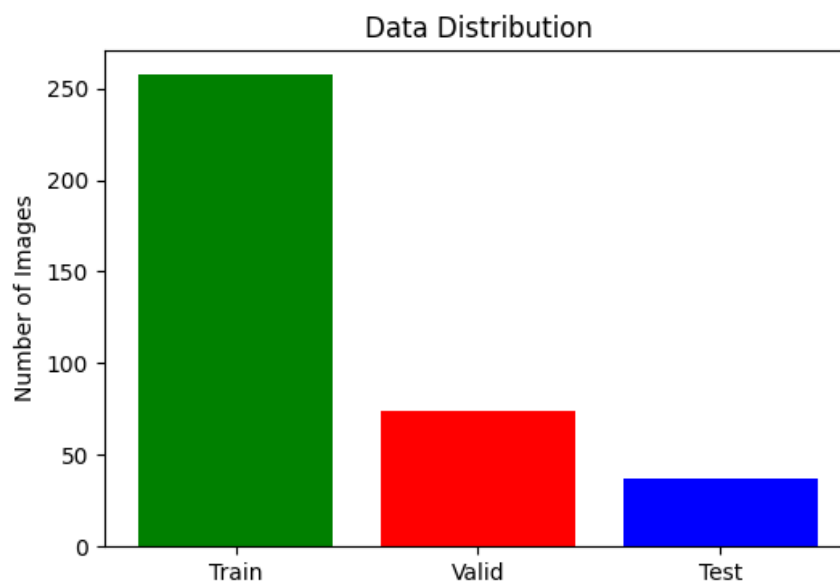


Figure 4.7: Dataset splitting: training, validation, and test sets.

4.3.3 Data Preprocessing

Before feeding MR volumes into our models, we apply a series of standardized preprocessing steps to ensure consistency and improve model robustness. Our pipeline operates on 2D axial slices extracted from 3D volumes, as follows:

1. **Slice Extraction.** For each patient volume, we select 100 consecutive axial slices starting at index 22. This avoids initial and final slices that contain little anatomical information.
2. **Resizing.**
 - *Image Slices:* Each extracted slice is resized to 128×128 pixels to match the U-Net input dimensions.

- *Segmentation Masks*: Corresponding ground-truth masks are first resized to 240×240 (to preserve label fidelity) and later downsampled alongside images during one-hot encoding.
3. **Intensity Normalization.** All pixel intensities in a slice are divided by the global maximum value of that volume, scaling inputs to the $[0, 1]$ range. This step harmonizes contrast across patients and modalities.
 4. **Augmentation.** To increase effective training diversity, random geometric transformations are applied during batch generation:
 - Horizontal and vertical flips (each with 50% probability).
 - Rotations by multiples of 90° (randomly chosen among $0^\circ, 90^\circ, 180^\circ, 270^\circ$).

4.4 Evaluation Metrics

To quantify the performance of our segmentation and classification models, we use a suite of metrics that assess accuracy, robustness, and specificity:

- **Accuracy**

$$\text{Accuracy} = \frac{\text{TP} + \text{TN}}{\text{TP} + \text{TN} + \text{FP} + \text{FN}}$$

- *Segmentation*: Proportion of correctly classified pixels (tumor vs. non-tumor).
- *Classification*: Proportion of correctly classified patients (LGG vs. HGG).

- **Precision** (Positive Predictive Value)

$$\text{Precision} = \frac{\text{TP}}{\text{TP} + \text{FP}}$$

- *Segmentation*: Fraction of predicted tumor pixels that are actually tumor.
- *Classification*: Fraction of patients predicted as HGG who truly have HGG.

- **Recall** (Sensitivity or True Positive Rate)

$$\text{Recall} = \frac{\text{TP}}{\text{TP} + \text{FN}}$$

- *Segmentation*: Fraction of actual tumor pixels correctly identified.
- *Classification*: Fraction of actual HGG patients correctly identified.

- **Specificity** (True Negative Rate)

$$\text{Specificity} = \frac{\text{TN}}{\text{TN} + \text{FP}}$$

- *Segmentation*: Fraction of non-tumor pixels correctly classified as non-tumor.
- *Classification*: Fraction of actual LGG patients correctly identified as LGG.

- **F1-Score**

$$\text{F1} = \frac{2\text{TP}}{2\text{TP} + \text{FP} + \text{FN}}$$

- *Classification*: Harmonic mean of precision and recall for each class, then averaged.

- **Intersection over Union (IoU)** Also called Jaccard index:

$$\text{IoU} = \frac{\text{TP}}{\text{TP} + \text{FP} + \text{FN}}$$

- *Segmentation*: Overlap between predicted and ground-truth tumor masks, averaged over classes (mIoU).

- **Dice Coefficient** (Segmentation F1)

$$\text{Dice} = \frac{2\text{TP}}{2\text{TP} + \text{FP} + \text{FN}}$$

- *Segmentation*: Emphasizes overlap; computed overall and per-class (necrotic, edema, enhancing).

- **Confusion Matrix** A contingency table of true vs. predicted labels:

	Predicted Positive	Predicted Negative
Actual Positive	TP	FN
Actual Negative	FP	TN

- *Classification*: Provides counts of TP, FP, FN, TN for LGG/HGG.

- **ROC AUC** (Area Under the Receiver Operating Characteristic Curve)

$$\text{AUC} = \frac{1}{2} \sum_{i=1}^n (\text{TPR}_i + \text{TPR}_{i-1}) \times (\text{FPR}_i - \text{FPR}_{i-1})$$

- *Classification*: Measures the trade-off between sensitivity and specificity across thresholds.

knowing that:

- TP = number of true positive cases (correctly predicted positive).
- TN = number of true negative cases (correctly predicted negative).
- FP = number of false positive cases (incorrectly predicted positive).
- FN = number of false negative cases (incorrectly predicted negative).
- TPR = true positive rate (recall): $\text{TPR} = \frac{\text{TP}}{\text{TP} + \text{FN}}$.
- FPR = false positive rate: $\text{FPR} = \frac{\text{FP}}{\text{FP} + \text{TN}}$.
- TNR = true negative rate (specificity): $\text{TNR} = \frac{\text{TN}}{\text{TN} + \text{FP}}$.
- FNR = false negative rate: $\text{FNR} = \frac{\text{FN}}{\text{FN} + \text{TP}}$.

4.5 Results and Discussion

4.5.1 Segmentation Results

In this section, we present the results of our U-Net segmentation model on the BraTS2020 dataset. The model was trained for 50 epochs with a batch size of 16, we will discuss the end results of the training and validation process, including loss and accuracy metrics.

4.5.1.1 Accuracy

The model achieved a pixel-level accuracy of 99.3%, demonstrating that the vast majority of pixels were correctly classified. The accuracy trend, illustrated in Figure 4.8, confirms stable and effective learning throughout the training process.

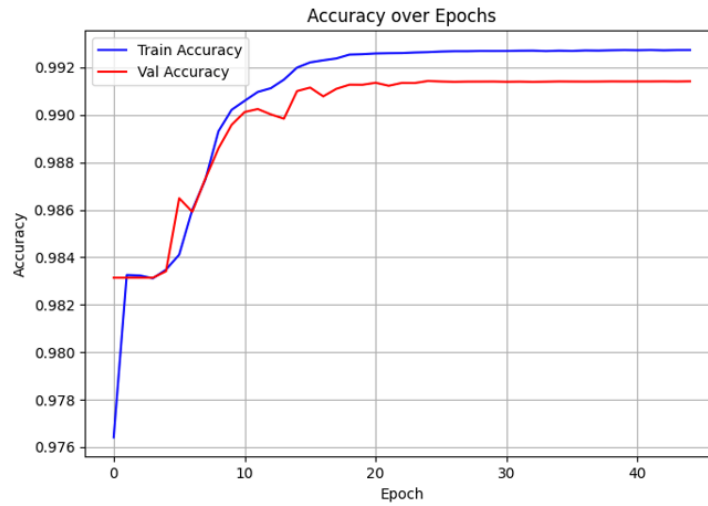


Figure 4.8: Training and Validation Accuracy over Epochs for the U-Net Segmentation Model

4.5.1.2 Loss

A final loss value of 0.0231 indicates a strong alignment between predictions and ground truth. As shown in Figure 4.9, the training and validation loss curves demonstrate smooth convergence, reflecting effective learning and minimal overfitting.

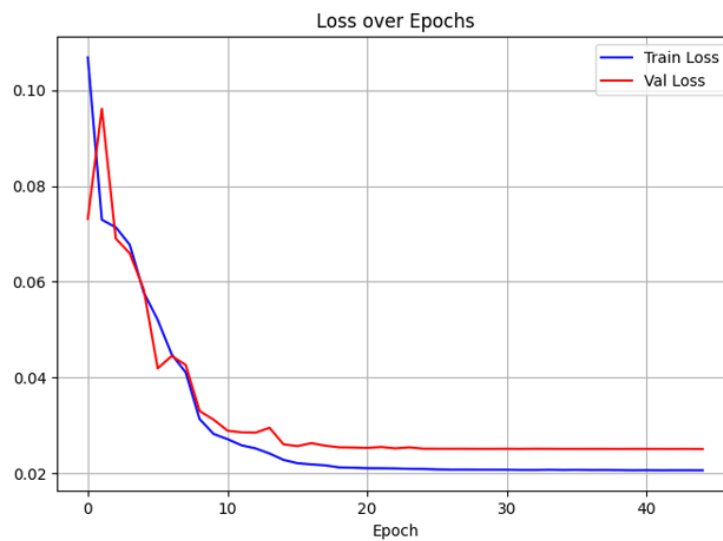


Figure 4.9: Training and Validation Loss over Epochs for the U-Net Segmentation Model

4.5.1.3 Dice Coefficient

The model achieved an overall Dice score of 58.98%, indicating a reasonable level of agreement between the predicted and ground truth tumor regions. Additionally, per-class Dice scores were computed to assess performance across specific tumor subregions. Figure 4.10 illustrates the training and validation Dice coefficient trends throughout the learning process.

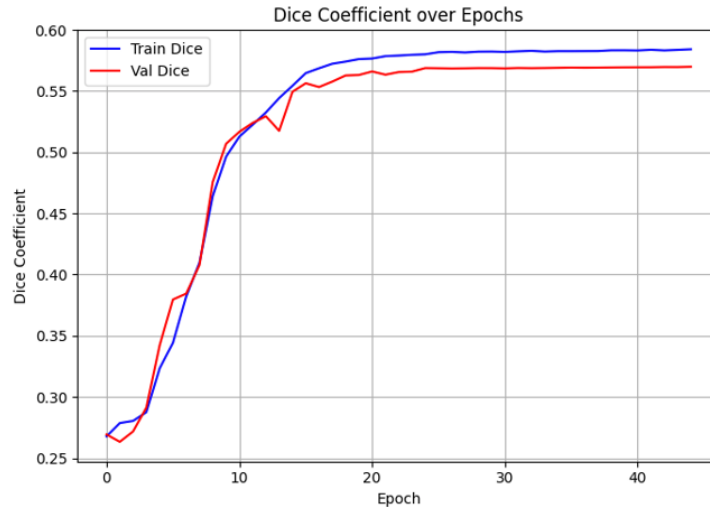


Figure 4.10: Training and Validation Dice Coefficient over Epochs for the U-Net Segmentation Model

4.5.1.4 Mean IoU

The model achieved a mean Intersection over Union (IOU) of 74.66%, reflecting a solid overlap between predicted and actual segmentation masks. Figure 4.11 illustrates the progression of training and validation IoU values, confirming consistent performance across classes.

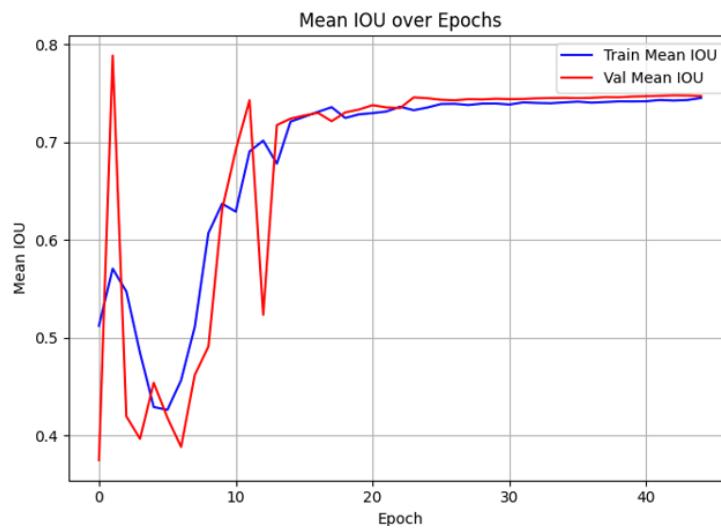


Figure 4.11: Training and Validation Mean IoU over Epochs for the U-Net Segmentation Model

Table 4.1: Performance Metrics for the U-Net Segmentation Model

Metric	Value
Loss	0.0231
Accuracy	99.30 %
Mean IoU	74.66 %
Dice Coefficient	58.98 %
Precision	99.37 %
Sensitivity	99.08 %
Specificity	99.79 %

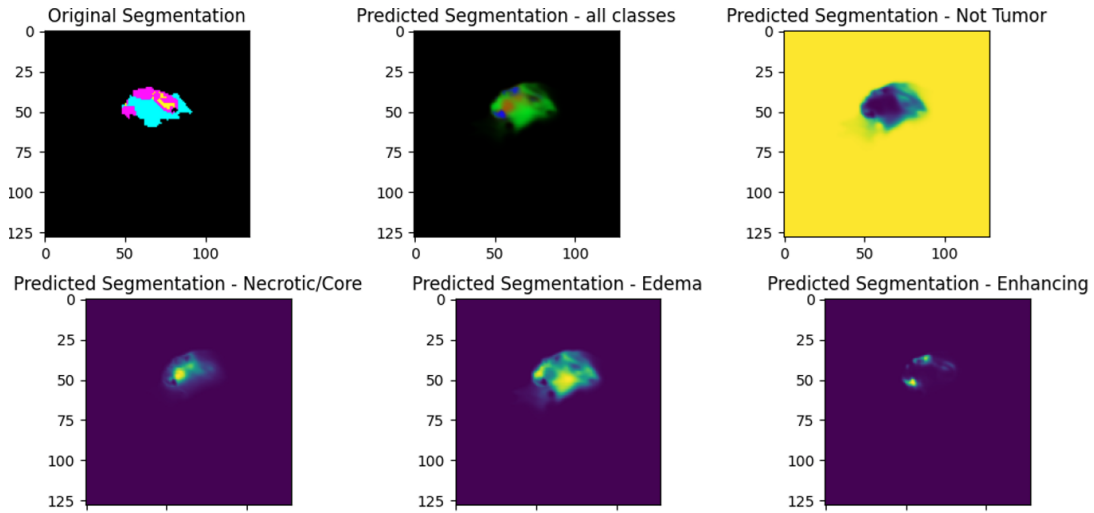


Figure 4.12: Sample of a Predicted tumor segmentation masks.

4.5.2 Classification Results

Table 4.2 summarizes the classification performance of the Support Vector Machine (SVM) model on the held-out test set. The model achieved an overall accuracy of 93.24 %, indicating strong generalization. High-grade gliomas (HGG) were classified with high precision (95 %) and recall (97 %), resulting in an F1-score of 96 %. In contrast, low-grade gliomas (LGG) achieved slightly lower metrics, with an F1-score of 83 %, reflecting a minor challenge in capturing the more subtle features associated with LGG.

The macro average shows a balanced view of precision and recall across both classes, with scores around 88–90 %, while the weighted average—which takes class support into account—remains consistent at 93 %. These results confirm the SVM model’s reliability and effectiveness in brain tumor grade classification, particularly in detecting HGG, which typically

has more distinct patterns and features.

Table 4.2: Performance Metrics of SVM Classifier on the Test Set

Class	Precision	Recall	F1-Score	Support
LGG (0)	86 %	80 %	83 %	15
HGG (1)	95 %	97 %	96 %	59
Accuracy	93.24 %			
Macro avg	90 %	88 %	89 %	74
Weighted avg	93 %	93 %	93 %	74

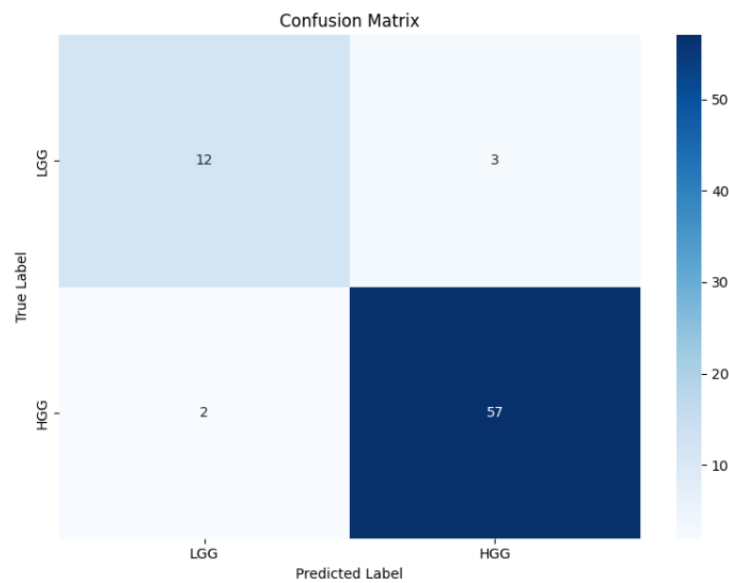


Figure 4.13: Confusion matrix for the SVM classifier.

4.6 Application Demo

To illustrate end-user interaction, we developed a lightweight demo application that integrates our trained U-Net and SVM models into a single GUI. The application consists of two main pages:

4.6.1 Upload Page

Presents an HTML form where the user can select and upload a brain tumor image (2D slice). Upon submission, the form sends a POST request to the `/results` route.

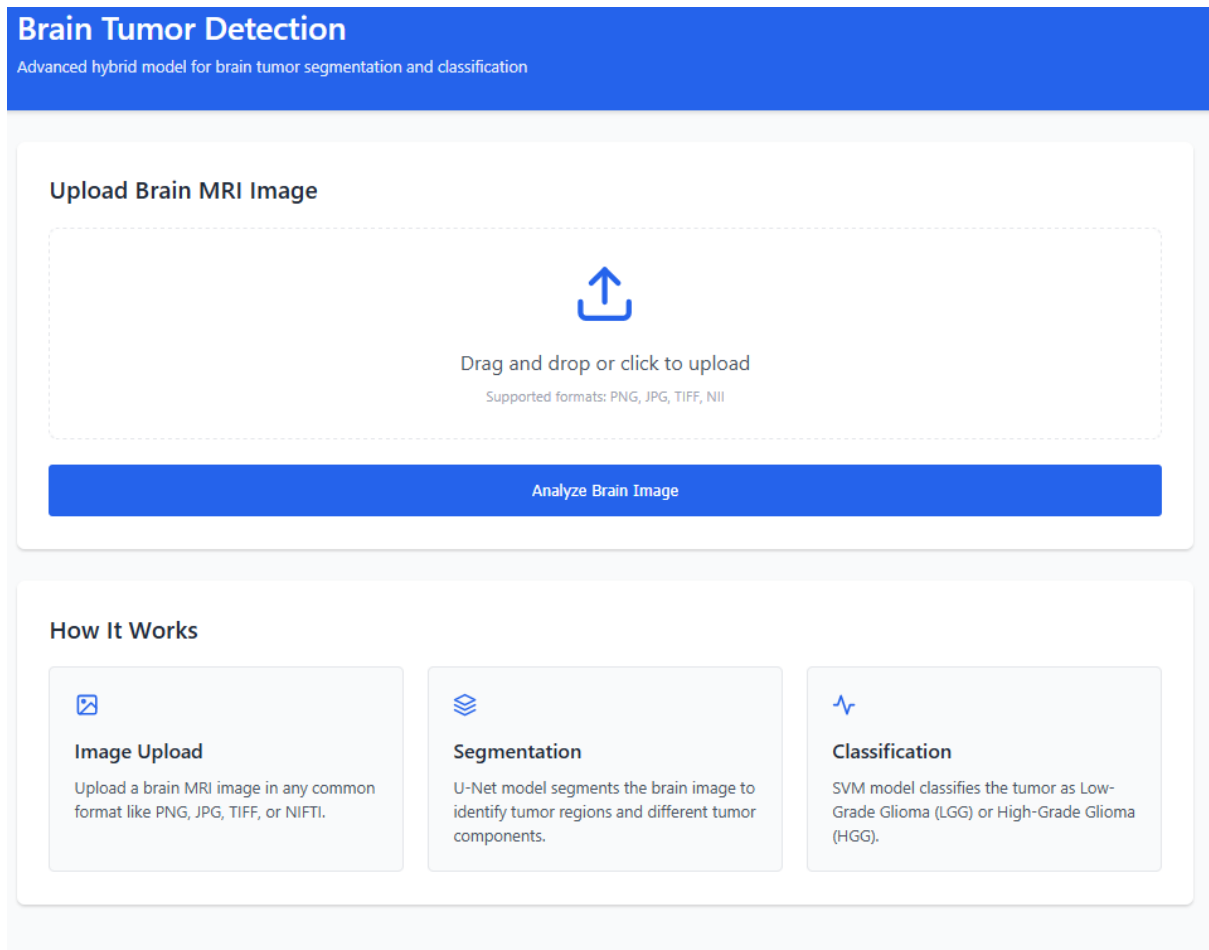


Figure 4.14: Upload page of the application demo.

4.6.2 Results Page

Receives the uploaded image, runs the preprocessing, segmentation (U-Net), feature extraction, and classification (SVM) pipeline, and then renders:

- The original input image.
- The segmentation mask overlaid on the input.
- The predicted tumor grade (LGG/HGG) with its confidence score.

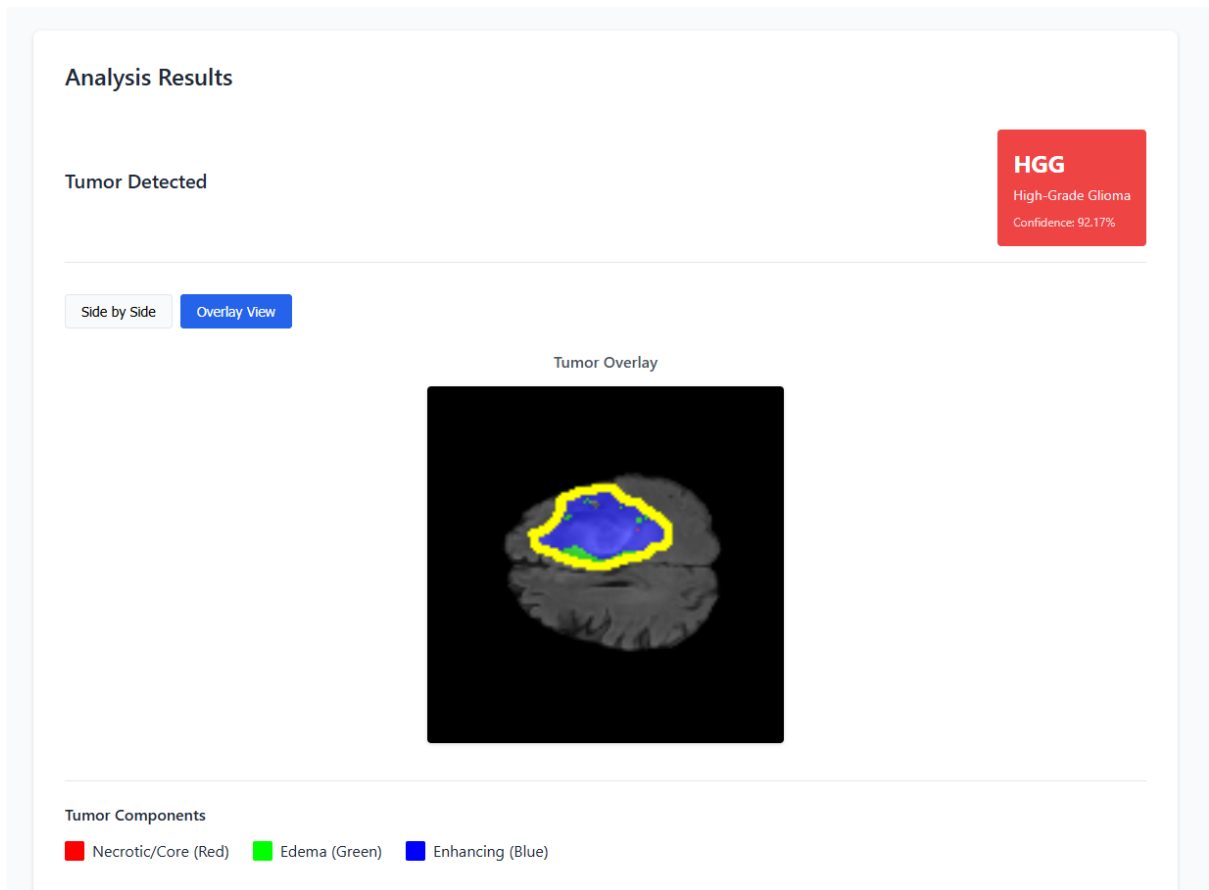


Figure 4.15: Results page of the application demo.

4.7 Conclusion

In this chapter, we have presented a comprehensive methodology for automated brain tumor detection and classification using MRIs. Our approach integrates a U-Net-based segmentation model with an SVM classifier, achieving high accuracy and robust performance across multiple evaluation metrics. The segmentation module demonstrated reliable delineation of tumor subregions, while the classification module effectively distinguished between high-grade and low-grade gliomas. Additionally, we showcased the practical application of our framework through a user-friendly demo application, highlighting its potential for real-world clinical use. These contributions underscore the effectiveness of combining deep learning and classical machine learning techniques in addressing complex medical imaging challenges.

General Conclusion

This thesis presents a hybrid framework for automated brain tumor detection and classification using MRI. By integrating deep learning and classical machine learning techniques, we demonstrate a robust and effective approach to addressing the challenges of brain tumor analysis.

Our framework, implemented using the BraTS2020 dataset, features two primary modules: a U-Net-based segmentation model and a Support Vector Machine classifier. The segmentation model achieved impressive pixel-level accuracy of 99.3%, a mean Intersection over Union (IoU) of 74.66%, and an overall Dice coefficient of 58.98%, while maintaining high specificity (99.79%) to avoid false positives. The classifier demonstrated strong performance with an overall accuracy of 93.24%, showing excellent capability in identifying high-grade gliomas (96% F1-score), which is particularly valuable given their more aggressive nature and need for urgent intervention. A key contribution of this work is the integration of these modules into an end-to-end pipeline, encapsulated in an intuitive, user-friendly demo application that allows medical professionals to upload patient images and rapidly receive diagnostic assistance.

While results are promising, challenges persist. Improving the Dice coefficient for intricate tumor subregions and enhancing classification, especially for low-grade gliomas (83% F1-score), are key. Future work should optimize segmentation, explore ensemble learning, expand datasets, implement 3D models, utilize attention mechanisms, validate externally, diversify tumor classification, and integrate explainable AI.

In conclusion, this thesis demonstrates the effectiveness of a hybrid framework combining deep learning and classical machine learning techniques for automated brain tumor analysis. The proposed framework advances the state of the art in tumor detection and classification and provides a practical tool that could assist radiologists in clinical settings.

Bibliography

- [1] C. Freudenrich, G. J. Tortora, and B. H. Derrickson, *Visualizing Anatomy and Physiology*. Wiley, 2013.
- [2] H. Sajedi and N. Pardakhti, “Age prediction based on brain mri image: a survey,” *Journal of Medical Systems*, vol. 43, no. 8, pp. 1–30, 2019.
- [3] South Jersey Radiology Associates. (2023, Oct.) What should i know about my brain mri results? Consulté le 10 mai 2025. [Online]. Available: <https://sjra.com/what-should-i-know-about-my-brain-mri-results/>
- [4] S. Thakkar. (2020, Feb.) Ai vs ml vs dl: What’s the difference? Accessed: 2025-05-09. [Online]. Available: <https://siddhithakkar.com/2020/02/24/ai-vs-ml-vs-dl-whats-the-difference/>
- [5] D. B. (2025) What is deep learning? Accessed: 2025-05-15. [Online]. Available: <https://www.alltius.ai/glossary/what-is-deep-learning>
- [6] GeeksforGeeks. (2025) Supervised and unsupervised learning. Accessed: 2025-05-15. [Online]. Available: <https://www.geeksforgeeks.org/supervised-unsupervised-learning/>
- [7] V. H. Phung and E. J. Rhee, “A high-accuracy model average ensemble of convolutional neural networks for classification of cloud image patches on small datasets,” *Applied Sciences*, vol. 9, no. 21, p. 4500, 2019. [Online]. Available: <https://www.mdpi.com/2076-3417/9/21/4500>
- [8] M. Oulmi and S. Kaloune, “Classification of objects with deep learning,” Master’s thesis, Akli Mohand Oulhadj University, Bouira, Algeria, 2018, master’s thesis.

- [9] O. Ronneberger, P. Fischer, and T. Brox, “U-net: Convolutional networks for biomedical image segmentation,” in *International Conference on Medical image computing and computer-assisted intervention*. Springer, 2015, pp. 234–241.
- [10] N. Wiest-Daesslé, “Imagerie du tenseur de diffusion pour l’étude de pathologies cérébrales,” Ph.D. dissertation, PhD thesis, Université, 2009.
- [11] G. J. Tortora and B. Derrickson, *Manuel d’anatomie et de physiologie humaines*. De Boeck Supérieur, 2017.
- [12] N. CHAKRAPARTYJ, “Brain mri images for brain tumor detection,” Kaggle dataset, accessed: 2022-01-21. [Online]. Available: <https://www.kaggle.com/datasets/navoneel/brain-mri-images-for-brain-tumor-detection>
- [13] R. J. Mackenzie, “Gray matter vs white matter,” Technology Networks – Neuroscience News and Research, 2019, accessed: 2022-03-21. [Online]. Available: <https://www.technologynetworks.com/neuroscience/articles/gray-matter-vs-white-matter-322973>
- [14] C. Analysis, “MedlinePlus [internet] – bethesda (md): National library of medicine,” Online, 2020, accessed: 2022-03-21. [Online]. Available: <https://medlineplus.gov/lab-tests/cerebrospinal-fluid-csf-analysis/>
- [15] D. Slimane, “Segmentation d’image médicale basées sur une coopération fcm et level set,” Ph.D. dissertation, Université Mouloud Mammeri, 2015.
- [16] M. A. Naser and M. J. Deen, “Brain tumor segmentation and grading of lower-grade glioma using deep learning in mri images,” *Computers in Biology and Medicine*, vol. 121, p. 103758, 2020.
- [17] T. S. Armstrong and et al., “Sleep-wake disturbance in patients with brain tumors,” *Neuro-oncology*, vol. 19, no. 3, pp. 323–335, 2017.
- [18] J. Bittoun, “Basic principles of magnetic resonance imaging,” in *SYLLABUS Methodology, Spectroscopy and Clinical MRI*, 1998, pp. 45–52.
- [19] B. H. Menze, A. Jakab, S. Bauer, J. Kalpathy-Cramer, K. Farahani, J. Kirby *et al.*, “The multimodal brain tumor image segmentation benchmark (BRATS),” *IEEE Transactions on Medical Imaging*, vol. 34, no. 10, pp. 1993–2024, 2015.

- [20] L. M. DeAngelis, “Brain tumors,” *New England Journal of Medicine*, vol. 344, no. 2, pp. 114–123, 2001.
- [21] ScienceDirect Topics, “Artificial intelligence – an overview,” <https://www.sciencedirect.com/topics/social-sciences/artificial-intelligence>, accessed: 2025-04-26.
- [22] J. Hurwitz and D. Kirsch, *Machine Learning For Dummies, IBM Limited Edition*. John Wiley & Sons, 2018.
- [23] S. Wang and R. M. Summers, “Machine learning and radiology,” *Medical Image Analysis*, vol. 16, no. 5, pp. 933–951, 2019.
- [24] S. Mortaheb, K. Oberijko, G. Kalinka *et al.*, “Machine learning approaches for the prediction of alzheimer’s disease from mri images: A systematic review,” *Journal of Alzheimer’s Disease*, vol. 70, no. 4, pp. 1159–1174, 2019.
- [25] P. Lambin, E. Rios-Velazquez, R. Leijenaar *et al.*, “Radiomics: Extracting more information from medical images using advanced feature analysis,” *European Journal of Cancer*, vol. 48, no. 4, pp. 441–446, 2012.
- [26] J. Futoma, J. Morris, and J. Lucas, “A comparison of models for predicting early hospital readmissions,” *Journal of Biomedical Informatics*, vol. 56, pp. 229–238, 2015.
- [27] P. Treleaven, M. Galas, and V. Lalchand, “Algorithmic trading review,” *Communications of the ACM*, vol. 56, no. 11, pp. 76–85, 2013.
- [28] F. Ricci, L. Rokach, B. Shapira, and P. B. Kantor, *Recommender Systems Handbook*. Springer, 2011.
- [29] W. Verbeke, K. Dejaeger, D. Martens, J. Hur, and B. Baesens, “New insights into churn prediction in the telecommunication sector: A profit driven data mining approach,” *European Journal of Operational Research*, vol. 218, no. 1, pp. 211–229, 2012.
- [30] R. Carbonneau, K. Laframboise, and R. Vahidov, “Application of machine learning techniques for supply chain demand forecasting,” *European Journal of Operational Research*, vol. 184, no. 3, pp. 1140–1154, 2008.
- [31] Y. Wu, T. Liu, E. Paredes *et al.*, “Real-time energy management in microgrids,” *IEEE Transactions on Smart Grid*, vol. 5, no. 2, pp. 810–819, 2014.

- [32] C. Cortes and V. Vapnik, "Support-vector networks," *Machine Learning*, vol. 20, no. 3, pp. 273–297, 1995.
- [33] L. Breiman, "Random forests," *Machine Learning*, vol. 45, no. 1, pp. 5–32, 2001.
- [34] I. Rish, "An empirical study of the naive bayes classifier," in *IJCAI 2001 Workshop on Empirical Methods in Artificial Intelligence*, vol. 3, no. 22, 2001, pp. 41–46.
- [35] T. M. Cover and P. E. Hart, "Nearest neighbor pattern classification," *IEEE Transactions on Information Theory*, vol. 13, no. 1, pp. 21–27, 1967.
- [36] D. C. Montgomery, E. A. Peck, and G. G. Vining, *Introduction to Linear Regression Analysis*. John Wiley & Sons, 2021.
- [37] R. Tibshirani, "Regression shrinkage and selection via the lasso," *Journal of the Royal Statistical Society: Series B (Methodological)*, vol. 58, no. 1, pp. 267–288, 1996.
- [38] C. E. Rasmussen and C. K. Williams, *Gaussian Processes for Machine Learning*. MIT Press, 2006.
- [39] J. MacQueen, "Some methods for classification and analysis of multivariate observations," *Proceedings of the Fifth Berkeley Symposium on Mathematical Statistics and Probability*, vol. 1, no. 14, pp. 281–297, 1967.
- [40] S. C. Johnson, "Hierarchical clustering schemes," *Psychometrika*, vol. 32, no. 3, pp. 241–254, 1967.
- [41] D. Shen, G. Wu, and H.-I. Suk, "Deep learning in medical image analysis," *Annual Review of Biomedical Engineering*, vol. 19, pp. 221–248, 2017.
- [42] N. Tajbakhsh, J. Y. Shin, S. R. Gurudu, R. T. Hurst, C. B. Kendall, M. B. Gotway, and J. Liang, "Convolutional neural networks for medical image analysis: Full training or fine tuning?" *IEEE Transactions on Medical Imaging*, vol. 35, no. 5, pp. 1299–1312, 2016.
- [43] N. M. Nguyen and N. Ray, "End-to-end learning of convolutional neural net and dynamic programming for left ventricle segmentation," in *Proceedings of the Third Conference on Medical Imaging with Deep Learning*, ser. Proceedings of Machine Learning Research, T. Arbel, I. Ben Ayed, M. de Bruijne, M. Descoteaux, H. Lombaert,

- and C. Pal, Eds., vol. 121. PMLR, 2020, pp. 555–569. [Online]. Available: <https://proceedings.mlr.press/v121/nguyen20a.html>
- [44] A. Krizhevsky, I. Sutskever, and G. E. Hinton, “Imagenet classification with deep convolutional neural networks,” in *Advances in Neural Information Processing Systems*, vol. 25, 2012, pp. 1097–1105.
 - [45] K. Simonyan and A. Zisserman, “Very deep convolutional networks for large-scale image recognition,” in *International Conference on Learning Representations*, 2015.
 - [46] K. He, X. Zhang, S. Ren, and J. Sun, “Deep residual learning for image recognition,” in *Proceedings of the IEEE Conference on Computer Vision and Pattern Recognition*, 2016, pp. 770–778.
 - [47] C. Szegedy, W. Liu, Y. Jia, P. Sermanet *et al.*, “Going deeper with convolutions,” in *Proceedings of the IEEE Conference on Computer Vision and Pattern Recognition*, 2015, pp. 1–9.
 - [48] G. Huang, Z. Liu, L. van der Maaten, and K. Q. Weinberger, “Densely connected convolutional networks,” in *Proceedings of the IEEE Conference on Computer Vision and Pattern Recognition*, 2017, pp. 4700–4708.
 - [49] O. Ronneberger, P. Fischer, and T. Brox, “U-net: Convolutional networks for biomedical image segmentation,” *Medical Image Computing and Computer-Assisted Intervention – MICCAI 2015*, pp. 234–241, 2015.
 - [50] S. Hochreiter and J. Schmidhuber, “Long short-term memory,” *Neural Computation*, vol. 9, no. 8, pp. 1735–1780, 1997.
 - [51] K. Cho, B. van Merriënboer, C. Gulcehre, D. Bahdanau *et al.*, “Learning phrase representations using rnn encoder-decoder for statistical machine translation,” in *Proceedings of the 2014 Conference on Empirical Methods in Natural Language Processing (EMNLP)*, 2014, pp. 1724–1734.
 - [52] A. Vaswani, N. Shazeer, N. Parmar, J. Uszkoreit *et al.*, “Attention is all you need,” in *Advances in Neural Information Processing Systems*, vol. 30, 2017, pp. 5998–6008.

- [53] I. J. Goodfellow, J. Pouget-Abadie, M. Mirza, B. Xu *et al.*, “Generative adversarial networks,” in *Advances in Neural Information Processing Systems*, vol. 27, 2014, pp. 2672–2680.
- [54] D. P. Kingma and M. Welling, “Auto-encoding variational bayes,” in *International Conference on Learning Representations*, 2014.
- [55] J. Ho, A. Jain, and P. Abbeel, “Denoising diffusion probabilistic models,” in *Advances in Neural Information Processing Systems*, vol. 33, 2020, pp. 6840–6851.
- [56] N. Parry, “Histology slide preparation: 5 important steps,” *Bitesize Bio*, 2024. [Online]. Available: <https://bitesizebio.com/13398/how-histology-slides-are-prepared/>
- [57] Leica Biosystems, “An introduction to specimen processing,” 2012. [Online]. Available: <https://www.leicabiosystems.com/us/knowledge-pathway/an-introduction-to-specimen-processing/>
- [58] —, “An introduction to routine and special staining,” 2012. [Online]. Available: <https://www.leicabiosystems.com/us/knowledge-pathway/an-introduction-to-routine-and-special-staining/>
- [59] Wikipedia contributors, “Histopathology,” *Wikipedia*, 2025. [Online]. Available: <https://en.wikipedia.org/wiki/Histopathology>
- [60] Raybloc, “Ultrasound, mri and ct scan – what’s the difference?” <https://raybloc.com/the-difference-ultrasound-mri-ct-scan/>, 2023, accessed: 2025-05-15.
- [61] Health Images, “Ct scan vs. mri: Differences, benefits, and risks,” <https://www.healthimages.com/mri-vs-ct-scan/>, 2019, accessed: 2025-05-15.
- [62] —, “Ct scan vs. mri: Differences, benefits, and risks,” <https://www.healthimages.com/mri-vs-ct-scan/>, 2019, accessed: 2025-05-15.
- [63] N. Elazab, W. Gab Allah, and M. Elmogy, “Computer-aided diagnosis system for grading brain tumor using histopathology images based on color and texture features,” *BMC Medical Imaging*, vol. 24, no. 1, p. 177, 2024. [Online]. Available: <https://bmcmmedimaging.biomedcentral.com/articles/10.1186/s12880-024-01355-9>

- [64] J. Barker, A. Hoogi, A. Depeursinge, and D. Rubin, "Automated classification of brain tumor type in whole-slide digital pathology images using local representative tiles," *Medical Image Analysis*, vol. 30, pp. 60–71, 2016. [Online]. Available: <https://www.sciencedirect.com/science/article/abs/pii/S1361841515001838>
- [65] S. A. Nishu, "Quantifying the defect visibility in digital images by proper color space selection," *International journal of engineering research and applications*, vol. 2, no. 3, pp. 1764–1767, 2012.
- [66] R. Yogamangalam, B. Karthikeyan *et al.*, "Segmentation techniques comparison in image processing," *International Journal of Engineering and Technology (IJET)*, vol. 5, no. 1, pp. 307–313, 2013.
- [67] M. A. Naser and M. J. Deen, "Brain tumor segmentation and grading of lower-grade glioma using deep learning in mri images," *Computers in Biology and Medicine*, vol. 121, p. 103758, 2020.
- [68] S. S. Begum and D. R. Lakshmi, "Combining optimal wavelet statistical texture and recurrent neural network for tumour detection and classification over mri," *Multimedia Tools and Applications*, pp. 1–22, 2020.
- [69] R. Hashemzahi, S. J. S. Mahdavi, M. Kheirabadi, and S. R. Kamel, "Detection of brain tumors from mri images base on deep learning using hybrid model cnn and nade," *Biocybernetics and Biomedical Engineering*, vol. 40, no. 3, pp. 1225–1232, 2020.
- [70] S. Kulkarni and G. Sundari, "A framework for brain tumor segmentation and classification using deep learning algorithm," *International Journal of Advanced Computer Science and Applications*, vol. 11, 2020.
- [71] Z. N. K. Swati, Q. Zhao, M. Kabir, F. Ali, Z. Ali, S. Ahmad, and J. Lu, "Brain tumor classification for mr images using transfer learning and fine-tuning," *Computerized Medical Imaging and Graphics*, vol. 75, pp. 34–46, 2019.
- [72] H. Dong, G. Yang, F. Liu, Y. Mo, and Y. Guo, "Automatic brain tumor detection and segmentation using u-net based fully convolutional networks," *arXiv preprint arXiv:1705.03820*, 2017. [Online]. Available: <https://arxiv.org/abs/1705.03820>

- [73] J. Walsh, A. Othmani, M. Jain, and S. Dev, “Using u-net network for efficient brain tumor segmentation in mri images,” *arXiv preprint arXiv:2211.01885*, 2022. [Online]. Available: <https://arxiv.org/abs/2211.01885>
- [74] S. Turk, K. Oguz, M. Orman, E. Caliskan, Y. Ertan, E. Ozgiray, T. Akalin, A. Srinivasan, and O. Kitis, “Machine learning based radiomics for glial tumor classification and comparison with volumetric analysis,” *arXiv preprint arXiv:2208.06739*, 2022. [Online]. Available: <https://arxiv.org/abs/2208.06739>
- [75] S. R. Gunn, “Support vector machines for classification and regression,” 1998. [Online]. Available: <https://api.semanticscholar.org/CorpusID:120347962>